

AD-A051 541

MECHANICAL TECHNOLOGY INC LATHAM N Y
MECHANICS OF ROLLER INSTABILITY IN ROLLER BEARINGS. (U)
JAN 78 P K GUPTA
MTI-78TR10

F/G 13/9

DAA629-77-C-0014

UNCLASSIFIED

ARO-14445.1-E

NL

1 OF 1
AD
A051541



END
DATE
FILMED
4 -78
DDC

ARO 14445.1-E

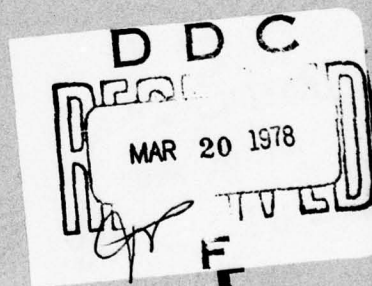
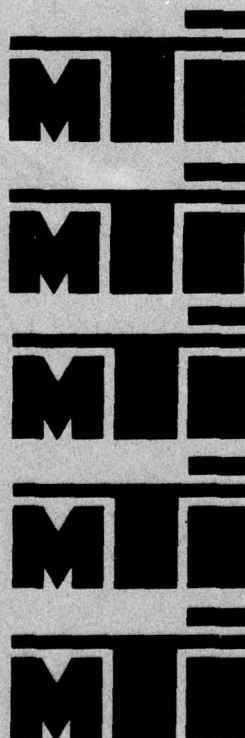
AD A051541

AD No.

DDC FILE COPY



12



DISTRIBUTION STATEMENT A
Approved for public release;
Distribution Unlimited

Mechanical Technology Incorporated

Research and Development Division

12

MTI 78TR10

MECHANICS OF ROLLER INSTABILITY
IN ROLLER BEARINGS

By:

Dr. Pradeep K. Gupta

Prepared for:

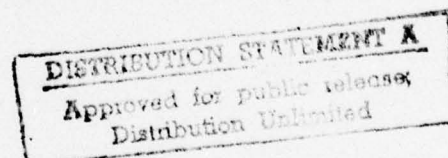
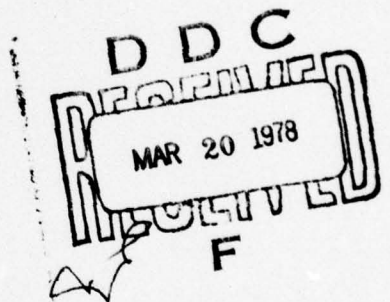
Army Research Office

Approved for public release;
distribution unlimited.

Prepared under:

Contract No. DAAG29-77-C-0014

January, 1978

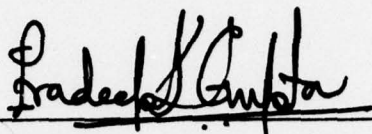


MECHANICAL TECHNOLOGY INCORPORATED
968 Albany-Shaker Road
Latham, New York 12110

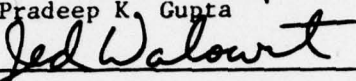
NO. MTI 78TR10

DATE: January 1978

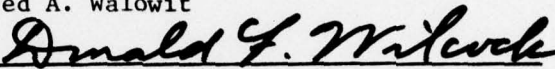
TECHNICAL REPORT
MECHANICS OF ROLLER INSTABILITY
IN ROLLER BEARINGS



Author (s) Pradeep K. Gupta



Approved Jed A. Walowit



Approved Donald F. Wilcock

Approved for public release; distribution unlimited.

Prepared for
Army Research Office

Prepared under
Contract No. DAAG29-77-C-0014



MECHANICAL TECHNOLOGY INCORPORATED

968 ALBANY - SHAKER ROAD - LATHAM, NEW YORK - PHONE 785-0922

18-ARJ
Unclassified

SECURITY CLASSIFICATION OF THIS PAGE (When Data Entered)

REPORT DOCUMENTATION PAGE		READ INSTRUCTIONS BEFORE COMPLETING FORM
1. REPORT NUMBER 19 14445.1-E	2. GOVT ACCESSION NO.	3. RECIPIENT'S CATALOG NUMBER
4. TITLE (and Subtitle) 6 Mechanics of Roller Instability in Roller Bearings.	5. PERFORMING ORG. REPORT NUMBER 14 MTI-78TR10	6. CONTRACT OR GRANT NUMBER(s) 5 DAAG29-77-C-0014 NEW
7. AUTHOR(s) 10 Pradeep K. Gupta	8. PERFORMING ORGANIZATION NAME AND ADDRESS Mechanical Technology Incorporated 968 Albany-Shaker Road Latham, New York 12110	9. PROGRAM ELEMENT, PROJECT, TASK AREA & WORK UNIT NUMBERS
11. CONTROLLING OFFICE NAME AND ADDRESS Army Research Office	12. REPORT DATE 11 Jan 1978	13. NUMBER OF PAGES 12-68p.
14. MONITORING AGENCY NAME & ADDRESS (if different from Controlling Office) Army Research Office	15. SECURITY CLASS. (of this report) Unclassified	15a. DECLASSIFICATION/DOWNGRADING SCHEDULE
16. DISTRIBUTION STATEMENT (of this Report) Approved for public release; distribution unlimited.		
17. DISTRIBUTION STATEMENT (of the abstract entered in Block 20, if different from Report)		
18. SUPPLEMENTARY NOTES The findings in this report are not to be construed as an official Department of the Army position, unless so designated by other authorized documents.		
19. KEY WORDS (Continue on reverse side if necessary and identify by block number) Roller Bearings Roller Instability in Rolling Bearings Roller Skidding Roller Skew High Frequency Motion in Roller Bearings		
20. ABSTRACT (Continue on reverse side if necessary and identify by block number) An analytical formulation for the roller motion in a cylindrical roller bearing is presented in terms of the classical differential equations of motion. Roller-race interaction is analyzed in detail and the resulting force and moment vectors are determined. Formulation for the roller end and race flange interaction during skewing of the roller is also considered. Elastohydrodynamic traction models for the turbo-33 type oil, 5P4E polyphenyl ether, and the MIL-L-7808 oil are summarized for the purpose of computing roller/race traction. The nature of the general motion of the roller is		

DD FORM 1 JAN 73 1473

EDITION OF 1 NOV 65 IS OBSOLETE

-iii-

SECURITY CLASSIFICATION OF THIS PAGE (When Data Entered)

224550

TC

Unclassified

SECURITY CLASSIFICATION OF THIS PAGE(When Data Entered)

20. investigated by integrating the equations of motion for a typical roller bearing. It is found that very high frequency vibrations in the roller motion result from the roller/race contact resonance.

ACCESSION for		
NTIS	White Section	<input checked="" type="checkbox"/>
DDC	B ff Section	<input type="checkbox"/>
UNANNOUNCED		<input type="checkbox"/>
JUSTIFICATION		
BY		
DISTRIBUTION/AVAILABILITY CODES		
Dist.	A	SPECIAL
A		

MECHANICS OF ROLLER INSTABILITY
IN ROLLER BEARINGS

by

Pradeep K. Gupta

ABSTRACT

An analytical formulation for the roller motion in a cylindrical roller bearing is presented in terms of the classical differential equations of motion. Roller-race interaction is analyzed in detail and the resulting force and moment vectors are determined. Formulation for the roller end and race flange interaction during skewing of the roller is also considered. Elastohydrodynamic traction models for the turbo-33 type oil, 5P4E polyphenyl ether, and the MIL-L-7808 oil are summarized for the purpose of computing roller/race traction. The nature of the general motion of the roller is investigated by integrating the equations of motion for a typical roller bearing. It is found that very high frequency vibrations in the roller motion result from the roller/race contact resonance.

TABLE OF CONTENTS

<u>Section</u>		<u>Page</u>
	REPORT DOCUMENTATION	-iii-
	ABSTRACT	-v-
	LIST OF FIGURES.	-viii-
	FOREWORD	-ix-
	LIST OF SYMBOLS.	-xi-
I	INTRODUCTION	I-1
II	GENERALIZED EQUATIONS OF ROLLER MOTION	II-1
III	ROLLER-RACE INTERACTIONS	III-1
IV	ROLLER END-RACE FLANGE INTERACTION	IV-1
V	ELASTOHYDRODYNAMIC TRACTION MODELS	V-1
VI	ROLLER MOTION RESULTS.	VI-1
VII	SUMMARY.	VII-1
VIII	RECOMMENDATIONS FOR FUTURE RESEARCH.	VIII-1
IX	REFERENCES	IX-1

LIST OF FIGURES

<u>Number</u>		<u>Page</u>
II-1	Coordinate Frames for Roller Motion	II-2
II-2	Transformations From The Inertial Frame (X,Y,Z) to Any Other Moving Frame (x_b, y_b, z_b)	II-5
III-1	Exaggerated View of Roller-Race Interaction	III-2
III-6	Roller-Race Contact Geometry.	III-6
IV-1	Sign Convention for Race Flange Angles.	IV-3
IV-2	Exaggerated View of Roller Corner and Race Flange Interaction .	IV-4
V-1	Hypothetical Traction Slip Relationship	V-2
V-2	Coordinate System in the Contact Ellipse.	V-10
V-3	Comparison of Actual and Simplified Traction Models at Low Temperature	V-16
V-4	Comparison of Actual and Simplified Traction Models at High Temperature	V-17
VI-1	Exaggerated View of the Bearing Model Used to Study the Roller Motion.	VI-3
VI-2	Roller/Race Contract Load Variation as the Roller Travels Through the Load Zone	VI-4
VI-3	Typical Roller Acceleration Profiles as it Travels Through the Load Zone	VI-5
VI-4	Roller/Race Slip and Traction Variations.	VI-7

FOREWORD

The work described herein was supported by the U.S. Army Research Office under Contract No. DAAG29-77-C-0014 with the directions of Dr. Edward Saibel of ARO, Durham, North Carolina, and Mr. Allen Royal of the U.S. Army Air Mobility R&D Lab, Ft. Eustis, Virginia.

LIST OF SYMBOLS

a, b	contact half widths
$[B]$	matrix defined by Equation (II.13)
d	roller diameter
E	Modulus of Elasticity
\vec{F}	applied force vector
\vec{F}_n	normal force vector
F_t	tractive force vector
G	Elasticity Parameter
G_1, G_2, G_3	Traction Parameters
\vec{G}	applied moment vector
\vec{G}_b	moment about the roller mass center
\vec{G}_r	moment about the race mass center
\vec{h}	angular momentum vector of the roller
$(\vec{i}, \vec{j}, \vec{k})$	unit vectors
$(\vec{I}, \vec{J}, \vec{K})$	unit vectors
I_1, I_2, I_3	principal moment of inertia for the roller
l	length coordinate along the roller length
m	roller mass
P_{Hz}	Hertzian Contact Pressure
Q	normal contact load
Q_m	Thermal Parameter
r	relative radial displacement of inner race
\vec{r}, \vec{R}	position vectors
\vec{r}_b	position vector locating the ball mass center in space
\vec{r}_{bg}	position vector locating the ball geometric center relative to its mass center
\vec{r}_{br}	position vector locating the ball geometric center relative to the race land center
\vec{r}_{brg}	position vector locating the roller geometric center relative to the race geometric center
\vec{r}_{gc}	position vector locating the race groove curvature center relative to the race geometric center

\vec{r}_p	position vector locating a point in the contact zone relative to the roller geometric center
\vec{r}_r	position vector locating the race mass center in space
\vec{r}_{rg}	position vector locating the race geometric center relative to its mass center
R	radius of the locus of roller corner centers of curvature
R_c	crown radius
R_{ce}	roller corner radius
R	radius of the circle representing the locus of race land centers (radius of race)
t	time
T_o	inlet temperature
$[T_{jk}]$	transformation matrix from frame j to frame k
$[T_{jk}]'$	transpose of $[T_{jk}]$
u	slip velocity
U	speed parameter
\vec{u}_b	roller velocity at any point in the contact ellipse
\vec{u}_r	race velocity at any point in the contact ellipse
\vec{u}_s	slip velocity at any point in the contact zone
v	rolling velocity
\vec{v}_b	translational velocity of roller mass center
\vec{v}_r	translational velocity of race mass center
w	load per unit length
W	load parameter
x	axial coordinate
(x,y,z)	race fixed coordinate frame
(x',y',z')	flange frame
(x _a ,y _a ,z _a)	azimuth frame
(x _b ,y _b ,z _b)	body fixed coordinate frame
(\bar{x},\bar{y},\bar{z})	contact frame
(\hat{x},\hat{y},\hat{z})	roller fixed coordinate frame
(X,Y,Z)	space fixed or inertial coordinate frame
α	pressure viscosity coefficient
α^*	apparent pressure-viscosity coefficient
β	temperature viscosity coefficient
β^*	apparent temperature viscosity coefficient

γ	race flange angle
δ	contact deflection
(η, β, γ)	transformation angle
θ	orbital coordinate
κ	traction coefficient
μ	viscosity
μ_o^*	apparent viscosity coefficient
ϕ	relative race misalignment
Φ	azimuth angle locating the ball center relative of the moving inner race center
χ	notation used for vector cross product
ψ	roller azimuth angle
ω	roller angular velocity
$\vec{\Omega}$	angular velocity of a coordinate frame
$\vec{\Omega}_1$	race angular velocity
ν	Poisson's Ratio

SECTION I

INTRODUCTION

Practical rotor systems subjected to relatively large radial loads are often supported by roller bearings primarily due to the large load support and stiffness characteristics of such bearing. A dominant radial load, however, causes a number of rollers to be completely unloaded as they travel in orbit. Thus, each roller is subjected to large load variations and, therefore, the resulting motion is somewhat complicated. Other factors such as irregular traction characteristics, roller-cage interactions, relative race misalignment, etc., further complicate the roller motion and sometimes lead to instabilities termed as "skidding" and "skewing". Skidding normally represents large sliding between the roller and the race, while skewing denotes rotation of the roller about its transverse axes. The primary objective of a bearing system design is to reduce or eliminate such instabilities under the prescribed operating conditions. A realistic design tool must simulate the roller motion with adequate generality in order to provide the required design guidelines. The development of such an analytical tool is the primary objective of the present investigation.

Most of the analytical simulations of roller bearing performance available to date have been restricted to quasi-static type of force balance models. It is clear that although such models will give adequate information about the overall load distribution and bearing fatigue life, they fail to provide any insight into the general motion of the roller and the resulting dynamic behavior of the bearing. For the simulation of even some of the simplest forms of roller motions, it is necessary that the general differential equations of motion be formulated and integrated in time, with prescribed initial conditions. The external forces on the roller are determined by the applied loads on the bearing, roller-race interaction models, lubricant traction behavior, roller-cage interactions and some other factors such as lubricant drag and churning.

This report contains the analysis relevant to the above general interactions in the case of a cylindrical roller bearing. The work is somewhat similar to an earlier investigation (reference 2) for the case of ball bearings. The motion of the cage, which is a crucial element for both ball and roller bearings, has also been

formulated in an earlier report. Thus, this report is the third part of a continuing project with the ultimate objective of developing generalized computer simulation models for the dynamic performance of both ball and roller bearings. The next forthcoming part, IV, will contain details about the traction models, churning losses and related factors. Some results of parametric studies will be described in Part V and Parts VI and VII will respectively be the user's manual and compilation listing of the computer program.

The generalized equations of motion for a cylindrical roller are described in the next section of this report. Sections III and IV are devoted to roller-race interactions and the race flange and roller end interaction. Simply for the purpose of computing the initial conditions for the general equations of motions, the static and quasi-static equilibrium equations are contained in Sections V and VI, respectively.

SECTION II

GENERALIZED EQUATIONS OF ROLLER MOTION

Similar to a ball bearing, the motion of a roller in a generalized simulation of the dynamic performance of a roller bearing can be considered in two parts:

- (1) Motion of the roller mass center in an inertial reference frame.
- (2) Rotational motion of the roller about its mass center.

A formulation of both the above parts of roller motion and a definition of the relevant coordinate frames will be the basic objectives of this section.

Motion of Ball Mass Center

As shown in Figure II-1, the translational motion of the roller center is best considered in a cylindrical coordinate frame, which is fixed in space and it, therefore, represents the inertial frame of reference. The classical differential equations of motion are written as

$$\ddot{x} = F_x/m$$

$$\ddot{r} - r\dot{\theta}^2 = F_r/m$$

$$r\ddot{\theta} + 2\dot{r}\dot{\theta} = F_{\theta}/m$$

where (F_x, F_r, F_{θ}) are components of the net applied forces on the roller and m is the mass of the roller.

For a given position of the roller mass center and all translational and angular velocities, the applied forces are calculated from the various interactions in the bearing, such as:

- Roller-race interaction
- Roller end - race flange interaction
- Roller-cage interaction
- Lubricant drag, churning or other interactions.

The mechanics of the roller-cage interaction have been formulated in (reference 1). The details of roller-race contact and the roller end - race flange interaction

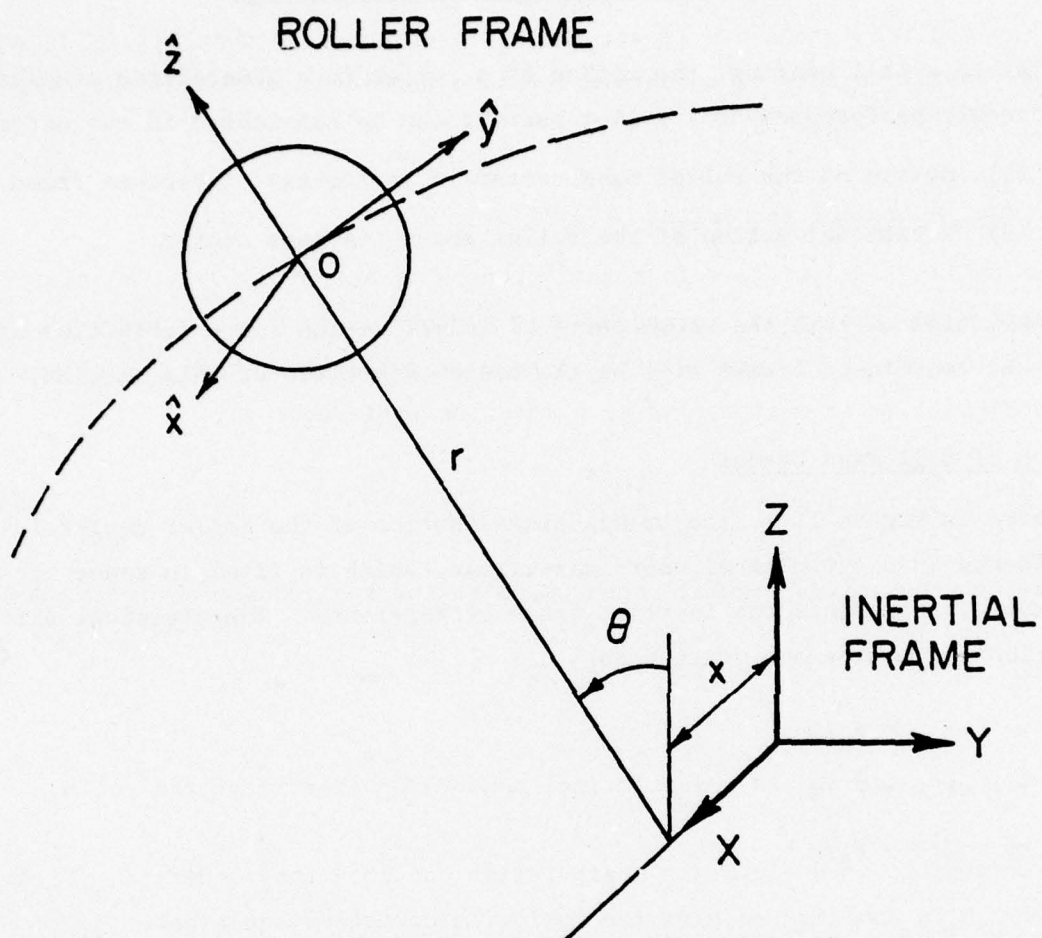


Figure II-1. Coordinate Frames for Roller Motion

will be considered in the next two sections of this report and other possible interactions will be undertaken as a part of future development.

Once the applied forces are known, the differential equations (II.1) of motion can be readily integrated to obtain the time dependent motion of the roller mass center.

Rotational Motion of the Roller

If the roller is considered to rotate about a fixed point, 0, with angular velocity $\vec{\omega}$ and the triad, formed by unit vectors \vec{i} , \vec{j} , \vec{k} along the principal axes of inertia at 0, rotates with an angular velocity $\vec{\Omega}$, then the classical differential equation of motion is written as (reference 7).

$$\dot{\vec{h}} = \frac{\delta \vec{h}}{\delta t} + \vec{\Omega} \times \vec{h} = \vec{G} \quad (\text{II.2})$$

where \vec{h} is the roller angular momentum, \vec{G} is the applied moment vector and

$$\frac{\delta \vec{h}}{\delta t} = I_1 \frac{d\omega_1}{dt} \vec{i} + I_2 \frac{d\omega_2}{dt} \vec{j} + I_3 \frac{d\omega_3}{dt} \vec{k} \quad (\text{II.3})$$

where I_1 , I_2 , and I_3 are the principal moments of inertia of the roller.

Some straightforward algebraic manipulation can show that equations (II.2) and (II.3) can be combined to give the following component equations:

$$\begin{aligned} I_1 \dot{\omega}_1 - I_2 \omega_2 \Omega_3 + I_3 \omega_3 \Omega_2 &= G_1 \\ I_2 \dot{\omega}_2 - I_3 \omega_3 \Omega_1 + I_1 \omega_1 \Omega_3 &= G_2 \\ I_3 \dot{\omega}_3 - I_1 \omega_1 \Omega_2 + I_2 \omega_2 \Omega_1 &= G_3 \end{aligned} \quad (\text{II.4})$$

In case of a "perfectly" cylindrical roller, the transverse moment of inertia

I_3 will be equal. However, this symmetry does not simplify the situation to any great extent since the polar axis has to be fixed in the roller. It will, therefore, be convenient to consider the roller angular motion in a roller fixed frame and preserve all generalities. A roller fixed frame will essentially mean that the triad of unit vectors \vec{i} , \vec{j} , \vec{k} , of equation (II.3) is fixed in the roller.

Thus, $\vec{\Omega} = \vec{\omega}$ and equations (II.4) reduce to the classical Euler equations of motion

$$\begin{aligned} I_1 \dot{\omega}_1 - (I_2 - I_3) \omega_2 \omega_3 &= G_1 \\ I_2 \dot{\omega}_2 - (I_3 - I_1) \omega_3 \omega_1 &= G_2 \\ I_3 \dot{\omega}_3 - (I_1 - I_2) \omega_1 \omega_2 &= G_3 \end{aligned} \quad (\text{II.5})$$

Clearly, the components of the moment vector \vec{G} will now be in the body fixed reference frame.

The applied moment vector \vec{G} is once again determined from the various interactions mentioned in the case of roller mass center motion. It is easy to understand that while the normal contact forces at each interaction dominate the mass center motion, the angular motion is dependent on the moments which result from the tractive forces at the various interactions.

Since the applied moments are conveniently expressed in the inertial coordinate frame, it will be necessary to define a law of transformation between the inertial and body fixed frames. Although such transformations have been defined in (reference 1) in case of the cage motion and in (reference 2) for ball motion, they will be repeated here for completeness.

Coordinate Transformations

As shown in Figure (II-2) let (X, Y, Z) be the inertial frame and (x_b, y_b, z_b) denote the body fixed frame. The required transformation is obtained in terms of three angles η , β , and γ by the following three successive rotations:

$$(i) \ \eta \vec{i}; \quad (ii) \ \beta \vec{j}; \quad (iii) \ \gamma \vec{k}_b$$

where $\vec{i}, \vec{j}, \vec{k}, \vec{i}_b, \vec{j}_b, \vec{k}_b$, etc. are unit vectors along the corresponding X, Y, Z , and x, y, z axes.

The relevant transformation from (X, Y, Z) to (x_b, y_b, z_b) frame may be written as

$$\vec{r}_b = [T_{ib}(\eta, \beta, \gamma)] \vec{R} \quad (\text{II.6})$$

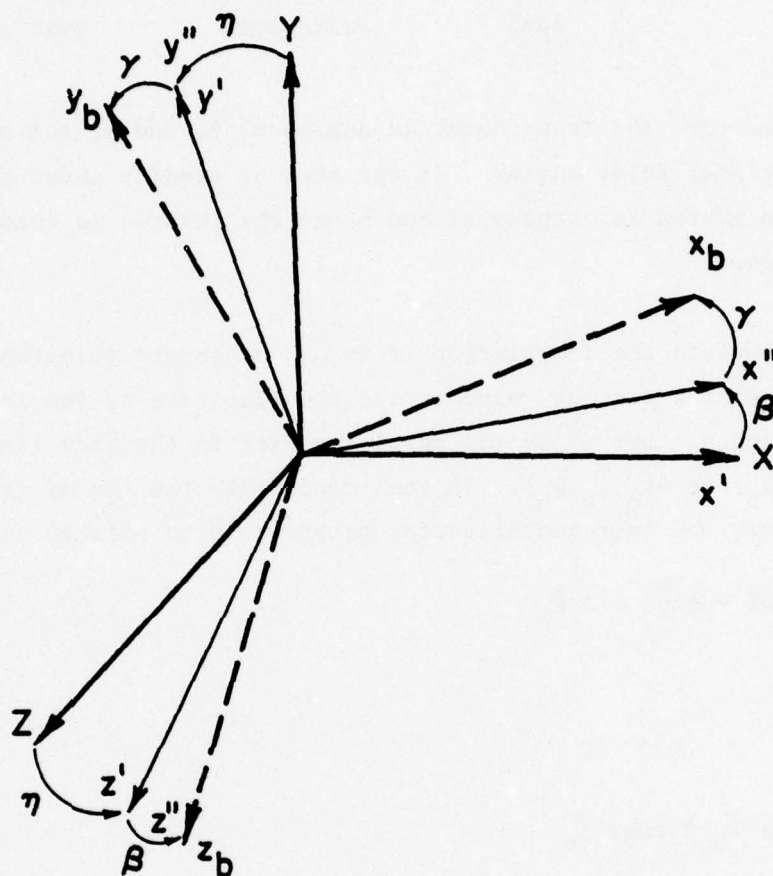


Figure II-2. Transformations From The Inertial Frame (X, Y, Z) to Any Other Moving Frame (x_b, y_b, z_b)

where

$$[T_{ib}(\eta, \beta, \gamma)] = \begin{bmatrix} \cos\beta \cos\gamma & \cos\eta \sin\gamma & \sin\eta \sin\gamma \\ -\cos\beta \sin\gamma & \cos\eta \cos\gamma & \sin\eta \cos\gamma \\ \sin\beta & -\sin\eta \cos\beta & \cos\eta \cos\beta \end{bmatrix} \quad (II.7)$$

It may be noted that the transformation angles η , β , and γ , are quite similar to the conventional Euler angles. It can also be readily shown that the above transformation matrix is orthogonal and hence the inverse is readily determined by the transpose.

In order to complete the formulation it is now necessary to establish the relationship between the angular velocity and the time rate of the transformation angles η , β , and γ . Let $\vec{\omega}^b$ be the angular vector in the body fixed reference frame (x_b, y_b, z_b) or $(\vec{i}_b, \vec{j}_b, \vec{k}_b)$. In accordance with the law of transformation defined earlier, the incremental vector rotation $\delta\vec{n}$ is written as

$$\delta\vec{n} = \Delta\eta\vec{i} + \Delta\beta\vec{j}' + \Delta\gamma\vec{k}_b \quad (II.8)$$

where

$$\vec{j}' = \sin\gamma \vec{i}_b + \cos\gamma \vec{j}_b$$

and

$$\begin{aligned} \vec{i} &= \cos\beta \vec{i}'' + \sin\beta \vec{k}_b \\ &= \cos\beta (\cos\gamma \vec{i}_b - \sin\gamma \vec{j}_b) + \sin\beta \vec{k}_b \end{aligned} \quad (II.9)$$

A combination of the above two equations results in the expression for required angular velocities

$$\begin{aligned} \delta\vec{n} &= (\Delta\eta\cos\beta\cos\gamma + \Delta\beta\sin\gamma)\vec{i}_b + (-\Delta\eta\cos\beta\sin\gamma + \Delta\beta\cos\gamma)\vec{j}_b + \\ &\quad (\Delta\eta\sin\beta + \Delta\gamma)\vec{k}_b \end{aligned}$$

or

$$\begin{Bmatrix} \omega_1^b \\ \omega_2^b \\ \omega_3^b \end{Bmatrix} = \begin{bmatrix} \cos\beta \cos\gamma & \sin\gamma & 0 \\ -\cos\beta \sin\gamma & \cos\gamma & 0 \\ \sin\beta & 0 & 1 \end{bmatrix} \begin{Bmatrix} \dot{\eta} \\ \dot{\beta} \\ \dot{\gamma} \end{Bmatrix} \quad (\text{II.10})$$

It may be noted that the matrix in Equation (II.10) is not orthogonal. However, the computation of the inverse is rather straightforward and some algebraic manipulation will show that

$$\begin{Bmatrix} \dot{\eta} \\ \dot{\beta} \\ \dot{\gamma} \end{Bmatrix} = \begin{bmatrix} \frac{\cos\gamma}{\cos\beta} & -\frac{\sin\gamma}{\cos\beta} & 0 \\ \sin\gamma & \cos\gamma & 0 \\ -\tan\beta \cos\gamma & \tan\beta \sin\gamma & 1 \end{bmatrix} \begin{Bmatrix} \omega_1^b \\ \omega_2^b \\ \omega_3^b \end{Bmatrix} \quad (\text{II.11})$$

The accelerations may be written by a straightforward differentiation of the above equation

$$\begin{Bmatrix} \ddot{\eta} \\ \ddot{\beta} \\ \ddot{\gamma} \end{Bmatrix} = \frac{\partial [\mathbf{B}]}{\partial t} \begin{Bmatrix} \omega_1^b \\ \omega_2^b \\ \omega_3^b \end{Bmatrix} + [\mathbf{B}] \begin{Bmatrix} \dot{\omega}_1^b \\ \dot{\omega}_2^b \\ \dot{\omega}_3^b \end{Bmatrix} \quad (\text{II.12})$$

where

$$[\mathbf{B}] = \begin{bmatrix} \frac{\cos\gamma}{\cos\beta} & -\frac{\sin\gamma}{\cos\beta} & 0 \\ \sin\gamma & \cos\gamma & 0 \\ -\tan\beta \cos\gamma & \tan\beta \sin\gamma & 1 \end{bmatrix} \quad (\text{II.13})$$

and it may be shown that

$$\frac{\partial [B]}{\partial t} \begin{bmatrix} -\dot{\gamma} \sin \gamma \sec \beta & -\dot{\gamma} \cos \gamma \sec \beta & 0 \\ +\dot{\beta} \cos \gamma \sec \beta \tan \beta & -\dot{\beta} \sin \gamma \sec \beta \tan \beta & 0 \\ \dot{\gamma} \cos \gamma & -\dot{\gamma} \sin \gamma & 0 \\ \dot{\gamma} \sin \gamma \tan \beta & \dot{\gamma} \cos \gamma \tan \beta & 0 \\ -\dot{\beta} \cos \gamma \sec^2 \beta & +\dot{\beta} \sin \gamma \sec^2 \beta & 0 \end{bmatrix} \quad (II.14)$$

For prescribed initial conditions the above formulation may be readily used to obtain the real time simulation of the ball motion. The initial conditions will consist of ball position and velocities. Thus, the mass center position, (x, r, θ) , mass center velocity, $(\dot{x}, \dot{r}, \dot{\theta})$, angular position, (η, β, γ) are prescribed at any instant of time. Sometimes $\vec{\omega}$ may be known instead of $(\dot{\eta}, \dot{\beta}, \dot{\gamma})$, in such a case equation (II.11) will provide the necessary relationship. With these given position and velocity components the force and moment vectors, \vec{F} and \vec{G} respectively, are computed from the models for the various interactions. Both these vectors will generally be determined in the inertial frame. The mass center accelerations are given by equation (II.1). For the angular acceleration the moment vector will have to be transformed in the roller fixed frame using equation (II.7) and (II.8). This transformed moment vector can then be substituted, along with the known angular velocities, in equations (II.4) and $\vec{\omega}$ can be determined. Equation (II.12) is now used to compute $\ddot{\eta}, \ddot{\beta}$ and $\ddot{\gamma}$. All the acceleration components are finally integrated numerically to obtain the required time dependent motion.

SECTION III

ROLLER-RACE INTERACTIONS

The normal and tractive forces at the roller-race contact constitute the dominant forces on the roller. The interaction is very similar to that in case of a ball-race contact (reference 2). It is first necessary to compute the geometrical interaction between the roller and a raceway. This geometrical interaction will define the elastic deflection, if a contact exists, which in turn will give the normal contact load, using a given load-deflection relationship. Once the contact geometry and load are determined, the local slip velocities in the contact zone may be determined from the prescribed velocities of the roller and race. A suitable traction model for a given lubricant and operating conditions is then used to compute the tractive force. A discussion of all these factors is the objective of this section.

Geometrical Considerations

Figure (III-1) schematically describes an exaggerated view of the geometrical interactions between the roller and a race. For simplicity, the diagram is drawn in the x-z plane and y axis is normal to the plane of the diagram. The position vector \vec{r}_r locates the mass center of the race, R_M , relative to the inertial frame (X,Y,Z). Vector \vec{r}_{rg} locates the race geometric center, R_G , relative to the mass center and vector \vec{r}_{gc} locates the center of race land R_L , relative to the race geometric center, R_G . Similarly the mass center of the roller, B_M , is located by \vec{r}_b relative to the inertial frame and \vec{r}_{bg} locates the roller geometric center relative to the mass center. The vectors \vec{r}_{rg} and \vec{r}_{bg} will generally be prescribed respectively in the race fixed frame (x,y,z) and the roller fixed frame ($\hat{x}, \hat{y}, \hat{z}$). Also, the relevant transformations will be:

Transformation from inertial to race frame: $[T_{ir}(\eta_r, \beta_r, \gamma_r)]$

Transformation from inertial to roller frame: $[T_{ib}(\eta_b, \beta_b, \gamma_b)]$

In addition to the above it will be convenient to define an azimuth frame (x_a, y_a, z_a) such that z_a is parallel to the radial component of \vec{r}_b , x_a is parallel to the inertial X axis and y_a is determined by the right-hand screw rule. Since the diagram in Figure (III-1) is drawn in the x-z plane, this coordinate frame is

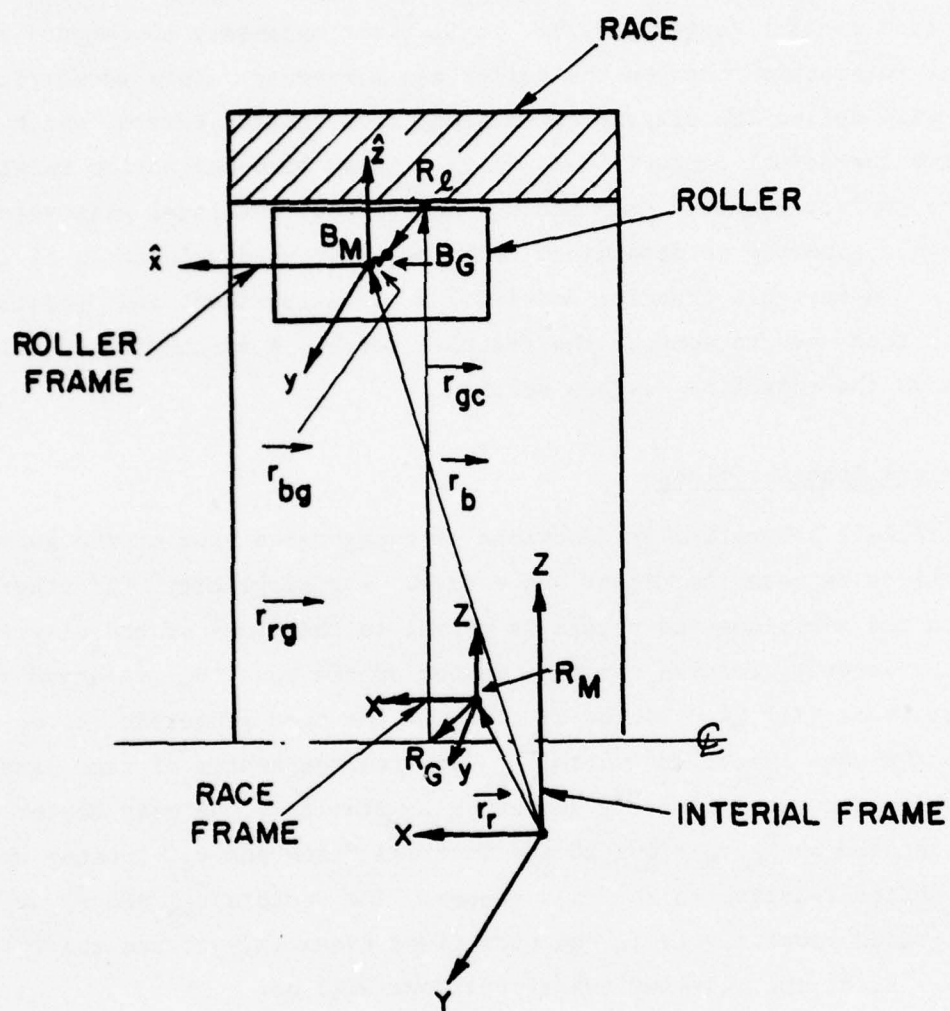


Figure III-1. Exaggerated View of Roller-Race Interaction

not shown in the figure. However, the transformation will depend only on the race azimuth angle Ψ , and it may be defined as

Transformation from inertial to roller azimuth frame: $[T_{1a}(\Psi, 0, 0)]$

In order to make the entire analysis applicable to both the outer and inner race contacts, it will be convenient to introduce a transformation from the azimuth to contact frame.

Transformation from azimuth to contact frame: $[T_{ac}(0, \alpha, 0)]$

where $\alpha = 0$ for outer race and π for inner race.

It may be noted that for most practical problems the mass and geometric centers may be coincident and this could simplify the geometry to some extent. The purpose of defining the geometric center different from the mass center is just to preserve the generality and capability of simulating some advanced configurations in the future.

Now the interaction between the roller and the race will be determined by locating the geometric center of the roller B_G , relative to the race land center, R_L . Let us denote this vector by \vec{r}_{br} and it will be given by the equation

$$\vec{r}_{br}^i = \vec{r}_b^i + [T_{1b}'] \vec{r}_{bg}^b - \left\{ \vec{r}_r^i + [T_{1r}'] (\vec{r}_{rg}^r + \vec{r}_{gc}^r) \right\} \quad (\text{III.1})$$

It may be noted that everything on the right-hand side of the above equation is known except for the vector \vec{r}_{gc}^r . It will be necessary to determine a race azimuth angle ϕ' , measured in the race fixed coordinate frame such that B_G , R_C , and R_G , all lie in one plane. The vector locating B_G , relative to R_G , \vec{r}_{brg} is written as

$$\vec{r}_{brg}^i = \vec{r}_b^i + [T_{1b}'] \vec{r}_{bg}^b - (\vec{r}_r^i + [T_{1r}'] \vec{r}_{rg}^r) \quad (\text{III.2})$$

When \vec{r}_{brg}^i is in the inertial frame, an angle ϕ' may be defined such that it denotes the angle between the inertial z axis and the plane containing vector \vec{r}_{brg}^i and a line passing through R_G and parallel to the inertial X axis.

Symbolically

$$\psi = \arctan \left(\frac{-r_{brg2}^i}{r_{brg3}^i} \right) \quad (III.3a)$$

If the race is assumed to be symmetric about the x axis, then the race fixed coordinate frame may not be necessary and $\phi' = \psi$. However, if the generalities mentioned above are preserved, then ϕ' , is determined in the race fixed frame such that \vec{r}_{gc} and \vec{r}_{brg} lie in the same plane. Now if R is the radius of the circle representing the locus of the race land centers, then

$$\vec{r}_{gc}^r = \{0, -R\sin\phi', R\cos\phi'\}$$

In order that \vec{r}_{gc} and \vec{r}_{brg} are coplaner, the y-component of the following vector must vanish

$$[T(\psi, 0, 0)] [T_{ir}'] \begin{Bmatrix} 0 \\ -R\sin\phi' \\ R\cos\phi' \end{Bmatrix} \quad (III.3b)$$

$$\text{or } \phi' = \arctan \left(\frac{T_{23}}{T_{22}} \right)$$

where T_{22} and T_{23} are the relevant components of the matrix obtained by the product $[T(\psi, 0, 0)] [T_{ir}']$.

Once ϕ' is known, \vec{r}_{br} may be determined in the inertial frame using equation (III.1) and it may be referenced in the race azimuth frame as

$$\vec{r}_{br}^a = [T(\phi', 0, 0)] \vec{r}_{br}^i \quad (III.4)$$

and in the contact frame

$$\vec{r}_{br}^c = [T_{ac}] \vec{r}_{br}^a \quad (III.5)$$

where the matrix $[T_{ac}]$ has already been defined above.

The computation of the roller azimuth ψ , is quite straightforward once the

orbital position, θ , locating the roller mass center is known from prescribed $\vec{r}_b \equiv (x, r, \theta)$ in cylindrical coordinates.

$$\psi = \theta - \arctan \frac{-r_2}{r_3} \quad (\text{III.6})$$

where r_2 and r_3 are the y and z components of the vector $[T_{ib}'] \vec{r}_{bg}$.

Once the geometric center of the roller is located relative to the race land center, it will be necessary to examine every point on the roller for possible interaction. Hence, the introduction of the roller geometry becomes essential at this point. Figure III-2 shows this geometry for a typical roller in a cylindrical roller bearing. The interaction between the roller and race will be restricted to the central flat land and the crowned areas at this point. Later in the next section the interaction between the roller end and race flange will be considered.

Now a point of the roller surface is best described in the roller frame by the position vector

$$\vec{r}^b = \begin{Bmatrix} -R' \sin \phi \\ R' \cos \phi \end{Bmatrix} \quad (\text{III.7})$$

Where ϕ is the angular position about the X axis, ℓ is the length coordinate along the X axis and R' is the effective radius. For the geometry shown in Figure III-2, will depend on ℓ

$$R' = \frac{d}{2}; \quad -\frac{L_2}{2} \leq \ell \leq \frac{L_2}{2}$$

$$\text{and } R' = \frac{d}{2} - \frac{L_2^2 - \ell^2}{4R_c} \quad -L_1 \leq \ell \leq -\frac{L_2}{2} \quad \text{and} \quad \frac{L_2}{2} \leq \ell \leq L_1$$

where R_c is the crown radius as shown in Figure III-2.

The vector \vec{r} can be expressed in the contact frame as

$$\vec{r}^c = [T_{ac}] [T_{ra}] [T_{ir}] [T_{ib}'] \vec{r}^b \quad (\text{III.8})$$

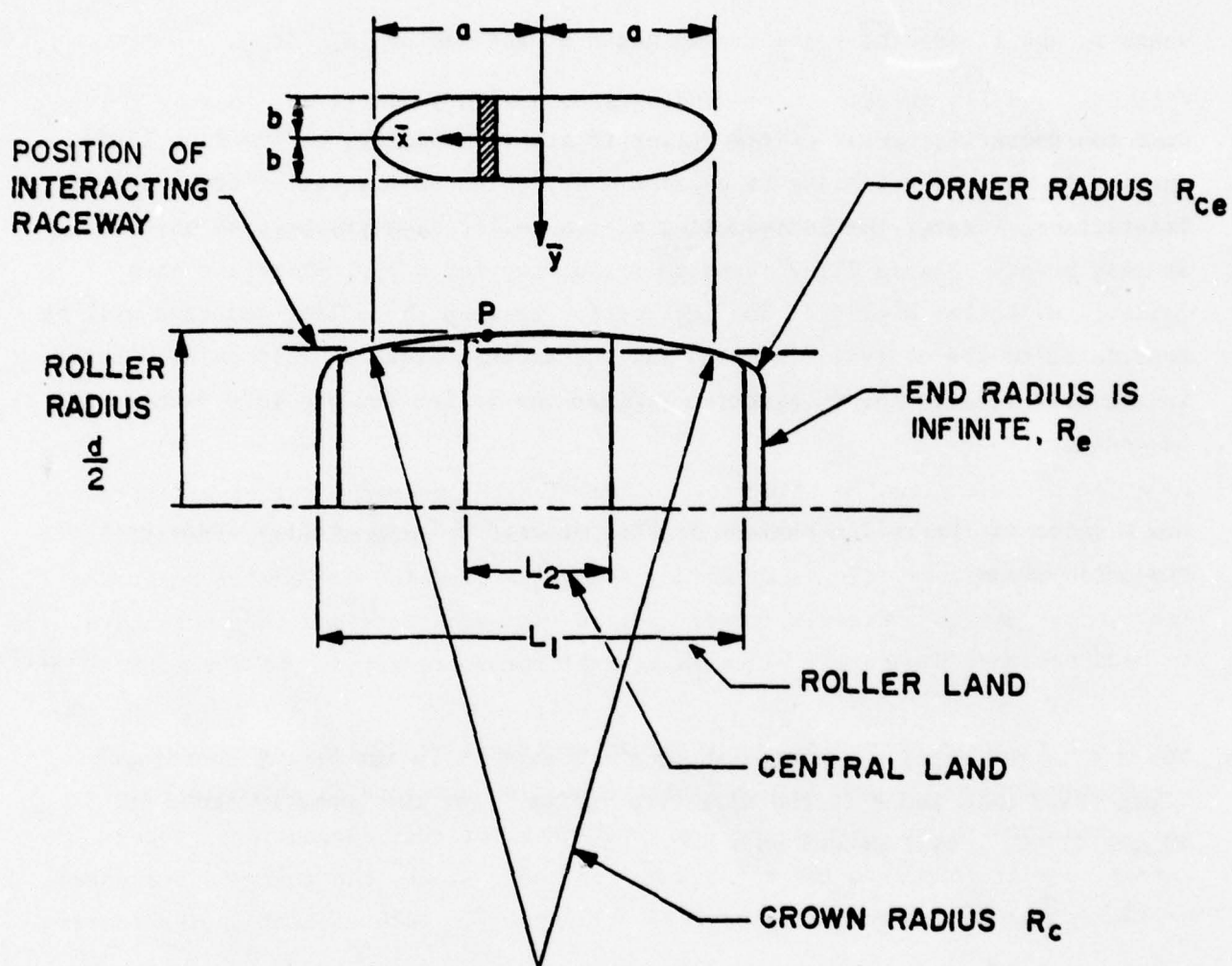


Figure III-2. Roller-Race Contact Geometry

For the point to be in the contact plane the y component of \vec{r}^c must vanish and this condition will determine the relevant ϕ . Since the rotation of the roller about the Y and Z axes will be in general small, it will only be necessary to compute ϕ for the roller center, hence

$$\phi = \arctan \frac{T_{23}}{T_{22}} \quad (\text{III.9})$$

where T_{23} and T_{22} are the corresponding elements in a matrix obtained by the product of matrices shown in equation (III.8).

The deflection at any point on the roller surface is now given as

$$\delta = (\vec{r}^c + \vec{r}_{br}^c)_3 \quad (\text{III.10})$$

A negative value of δ will mean no contact.

In order to determine the effective contact length, when the roller is crowned, the length coordinate l in equation (III.10) will be determined by standard bisection techniques. In other words, the value of l for $\delta = 0$ will determine the contact length. Clearly, these will be two such roots and they both have to be determined separately since in general the roots may not be symmetric.

For the purpose of computing the total interaction, it will be convenient to divide the contact length into a finite number of elements as shown in Figure III-2 and compute the normal and tractive loads for each element. A proper summation will then give the total required load. Thus, the analysis presented below for the normal and tractive load will apply to each element in the contact zone.

Normal Contact Load

The load deflection relation for a line contact is not uniquely defined, as in case of point contact. The deflection can be computed only in terms of strains corresponding to finite lengths in the two interacting bodies. (Reference 3) suggests a relationship of the form

$$\delta = \frac{2Q}{\pi l} \left[\frac{1-\nu_1^2}{E_1} \left\{ \ln \frac{2d_1}{b} - \frac{\nu_1}{2(1-\nu_1)} \right\} + \frac{1-\nu_2^2}{E_2} \left\{ \ln \frac{2d_2}{b} - \frac{\nu_2}{2(1-\nu_2)} \right\} \right] \quad (\text{III.11})$$

where the contact half width

$$b = \left\{ \frac{4Q}{\pi \ell \Sigma \rho} \left[\frac{1-\nu_1^2}{E_1} + \frac{1-\nu_2^2}{E_2} \right] \right\}^{\frac{1}{2}} \quad (\text{III.12})$$

ν_1, E_1, ν_2, E_2 , are the Poisson's ratio and elastic modulus for the two interacting bodies, $\Sigma \rho$ is the sum of the principal curvatures, Q is the normal contact load, and ℓ is the contact length.

The determination of lengths d_1 and d_2 is rather arbitrary and, hence, application of (III.11) becomes a little difficult.

In view of this difficulty, Lundberg (reference 4) has determined an empirical equation based on actual load deflection measurements in line contact. This relation is

$$\delta = \frac{2Q}{\pi \ell} \left[\frac{1-\nu_1^2}{E_1} + \frac{1-\nu_2^2}{E_2} \right] \left[\ln \frac{\ell}{b} + 1.1932 \right] \quad (\text{III.13})$$

where the contact half width b is given by equation (III.12).

It is clear that for a given Q , the computation of δ is straightforward from equation (III.13). However, when δ is prescribed, some type of iterative procedure will be necessary in order to compute Q .

Palmgren (reference 5) gives a relation which is free of the above difficulty.

$$\delta = 0.39 \left[\frac{4(1-\nu_1^2)}{E_1} + \frac{4(1-\nu_2^2)}{E_2} \right]^{0.90} \frac{Q^{0.90}}{\ell^{0.80}} \quad (\text{III.14})$$

In terms of results, the above two relations are fairly close. Hence, if equation (III.13) is to be used, then the initial guess in the iterative scheme can be derived from equation (III.14) and under such conditions the iteration will converge rather rapidly.

Tractive Forces and Moments

For the purpose of computing the traction, it will be necessary to define the

position vector locating the center of the elementary strip in the contact zone, relative to the roller mass center and the local slip velocities. If we assume that both roller and race deform equally, which is quite reasonable, then the required position vector may be written as

$$\vec{r}_p^{+b} = \begin{Bmatrix} \ell \\ -(R-\delta/2)\sin\phi \\ (R-\delta/2)\cos\phi \end{Bmatrix} \quad (\text{III.15})$$

In order to compute the local slip velocities, let the race have a translation velocity \vec{v}_r and an angular velocity $\vec{\omega}_r$. Likewise, let the roller have a translational velocity \vec{v}_b and an angular velocity $\vec{\omega}_b$. Generally, the angular velocities are specified in the body fixed frames while the translational velocities are measured in the inertial frame. Furthermore, the roller velocity is conveniently measured in the cylindrical coordinate frame in terms of components \dot{x} , \dot{r} , and $\dot{\theta}$. In terms of these components, the local slip velocity \vec{u}_s of the race relative to the roller at point P (see Figure III-2) is given in the contact frame in terms of the race and roller velocities, \vec{u}_r and \vec{u}_b respectively as

$$\vec{u}_r^c = [T_{ac}][T_{ia}] \left\{ \vec{v}_r^i + \left\{ [T_{ir}'] \vec{\omega}_r^r - \begin{Bmatrix} \dot{\theta} \\ 0 \\ 0 \end{Bmatrix} \right\} \times \left\{ \vec{R}_p^i + [T_{ir}'] \vec{r}_{rg}^r \right\} \right\} \quad (\text{III.16})$$

$$\vec{u}_b^c = [T_{ac}] \left\{ \begin{Bmatrix} \dot{x} \\ 0 \\ \dot{r} \end{Bmatrix} \right\} + [T_{ia}] \left\{ [T_{ib}'] \vec{\omega}_b^b \times \left\{ [T_{ia}'] [T_{ac}'] \vec{r}_p^c + [T_{ib}'] \vec{r}_{bg}^b \right\} \right\} \quad (\text{III.17})$$

$$\vec{u}_s^c = \vec{u}_r^c - \vec{u}_b^c \quad (\text{III.18})$$

where the vector \vec{R}_p , which locates the center of elementary strip with respect to the race mass center, is computed as

$$\vec{R}_p = \vec{r}_p + \vec{r}_{bg} + \vec{r}_b - (\vec{r}_r + \vec{r}_{rg}) \quad (\text{III.19})$$

The components u_{s1}^c and u_{s2}^c in the contact frame will result in traction, u_{s2}^c being along the rolling direction and u_{s1}^c being normal to it.

In case of a roller bearing the slip will be primarily in the y direction and, hence, the tractive force will act along the y axis. The relevant traction coefficient, κ , will be determined by the appropriate traction model, which will

be described in Section V, for the present it may be denoted as:

$$\kappa_2 = \kappa_2(u_2) \quad (\text{III.20})$$

where the subscript 2 is used to denote the y direction.

The tractive force, F_t , is now defined as

$$F_t = \kappa Q \quad (\text{III.21})$$

where Q is the already known normal load on the elementary strip.

Both the normal and tractive forces, acting on the roller can be combined in a general force vector, written conveniently in the contact frame as

$$\vec{F}^c = \begin{Bmatrix} 0 \\ \kappa Q \\ -Q \end{Bmatrix}$$

The force on the race will just be $-\vec{F}$, while the moments on the roller and race are defined as

$$G_b^{\rightarrow} = (r_p^{\rightarrow} + r_{bg}^{\rightarrow}) \times \vec{F}$$

$$\text{and } G_r^{\rightarrow} = (R_p^{\rightarrow} + r_{rg}^{\rightarrow}) \times \vec{F}$$

All vectors must be transformed to appropriate coordinate frames. It is convenient to compute the forces in the initial frame and the moments in a body fixed frame.

It should be remembered that all the above forces and moments will be on a given elementary strip in the contact zone and a summation over the contact zone will give the total force and moment vectors.

SECTION IV

ROLLER END-RACE FLANGE INTERACTION

In a roller bearing subjected to a slight misalignment, the loads between the roller and raceways may be somewhat nonsymmetric and, hence, the resulting tractions develop a moment about the transverse axis of the roller. Such a moment will lead to angular rotation of the roller about its transverse axis and this type of motion, which is highly undesirable, is generally called skewing. It is quite easy to understand that when the roller skews, the corners of the roller could interact with the cage and the flanges on the race. Generally, the axial clearance between the roller end and cage is quite large compared to that between the roller end and race flange. Hence, the cage interaction can be neglected, but it is essential that the roller end and race flange interaction be modelled in a realistic fashion in order to treat the roller skewing with adequate justice. Unfortunately, the local geometry and the kinematics greatly complicate the problem and the development of a realistic model becomes extremely difficult. It should be remembered that a realistic model should not only simulate the problem correctly, but it should also be simple enough to be rapidly executable of a digital computer, since computer time is a key factor in sophisticated programs, such as the one under consideration.

With the above difficulties in view, a first order interaction model for the roller end and race flange contact is derived on the basis of the following two assumptions:

- (1) If the roller end is not contacting the race flange, there is no contact force. In other words, any hydrodynamic action is neglected.
- (2) When the race flange is contacting the roller corner, which will have a finite radius of curvature, the contact load is approximated by an effective Hertzian type contact model and the tractive force is determined by a prescribed traction-slip relation.

It is, therefore, clear that the objective is to treat metal to metal contact only. There will basically be two parts to such a treatment, e.g., the contact geometry and the load deflection relationship. Both of these parts will be discussed in this section.

Geometrical Consideration

The roller geometric center was located with respect to the race geometric center in the preceeding center. In case of the roller corner and flange interaction, it will be necessary to locate the center of curvature of the roller corner with respect to a point on the race flange. Thus, an additional transformation from the race azimuth to flange frame is introduced.

Transformation from race azimuth to race flange frame: $(T_{rf} (0, \gamma, 0))$ where the angle γ will depend on the particular flange under consideration as shown, in an exaggerated fashion, in Figure IV-1.

It should also be noted that the race azimuth angle will now be defined by the relevant center of curvature of the roller corner and not by the center of roller.

Let us consider a point, 0, on the locus of the center of curvatures of the roller corner, as shown in Figure IV-2. It is clear that the locus will be a circle and the position vector locating 0, with respect to the roller geometric center in roller frame, is given as

$$\vec{r}_e^b = \begin{Bmatrix} \pm l \\ -R \sin \phi \\ R \cos \phi \end{Bmatrix} \quad (IV.1)$$

where ϕ is just angular coordinate about the X axis in the roller fixed frame.

It will be necessary to write \vec{r}_e^b in the race frame, and ultimately in the flange frame, and, hence, we recall the transformation from the roller to race frame from the preceeding section

$$[T_{br}] = [T_{ir}] [T_{ib}] \quad (IV.2)$$

Also, a vector \vec{r}_{brg} locating the roller geometric center with respect to the race geometric center can be written in terms of the various vectors introduced in Figure III-1 in the preceeding section.

$$\vec{r}_{brg} = [T_{ir}] \left\{ \vec{r}_b^i + [T_{ib}] \vec{r}_{bg}^b \right\} - \left\{ [T_{ir}] \vec{r}_r^i + \vec{r}_{rg}^r \right\} \quad (IV.3)$$

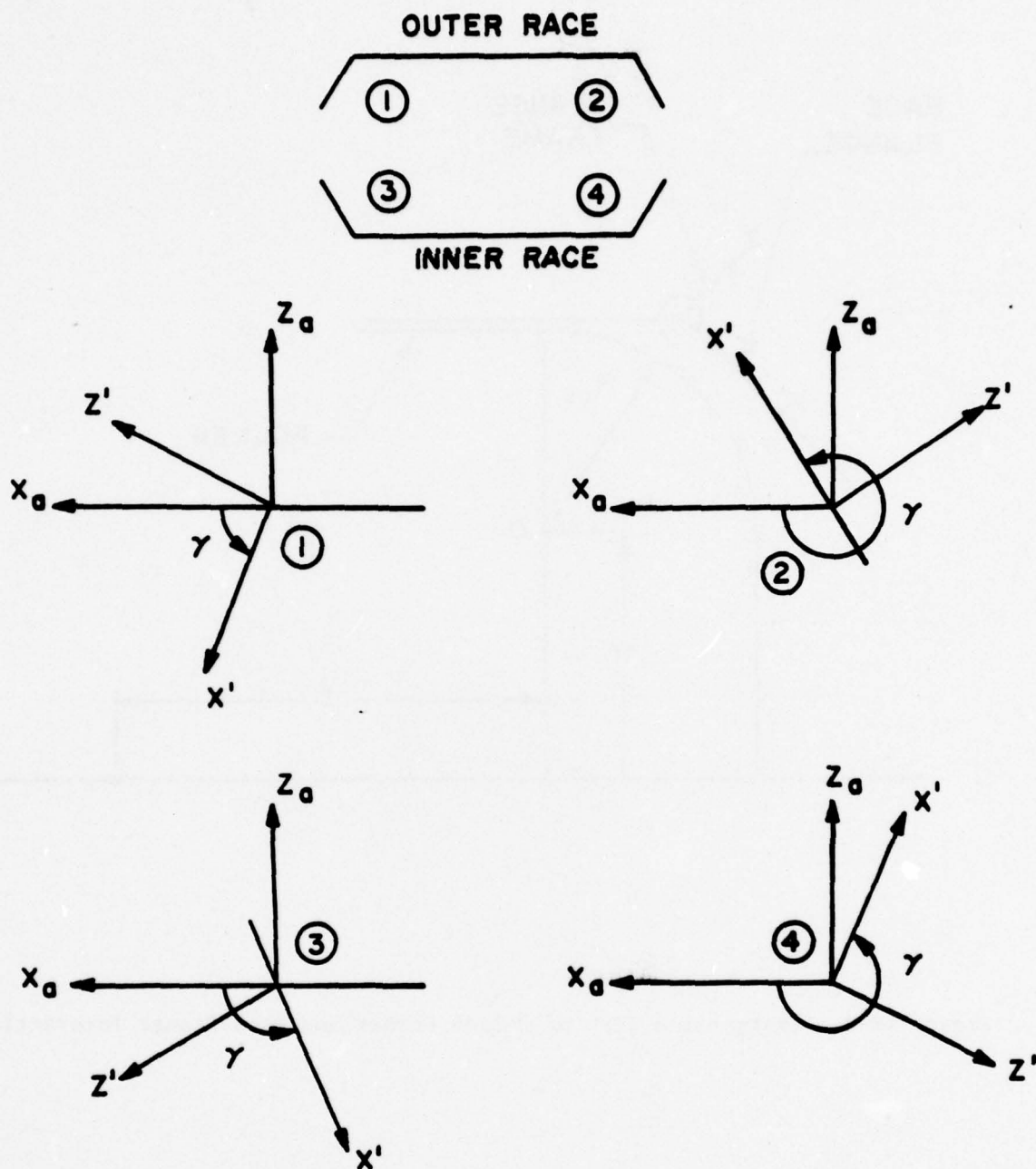


Figure IV-1. Sign Convention for Race Flange Angles. (X_a, Y_a, Z_a) is the race azimuth frame and (X', Y', Z') is the flange frame. Y axis is not shown since the figure is drawn in the X-Z plane.

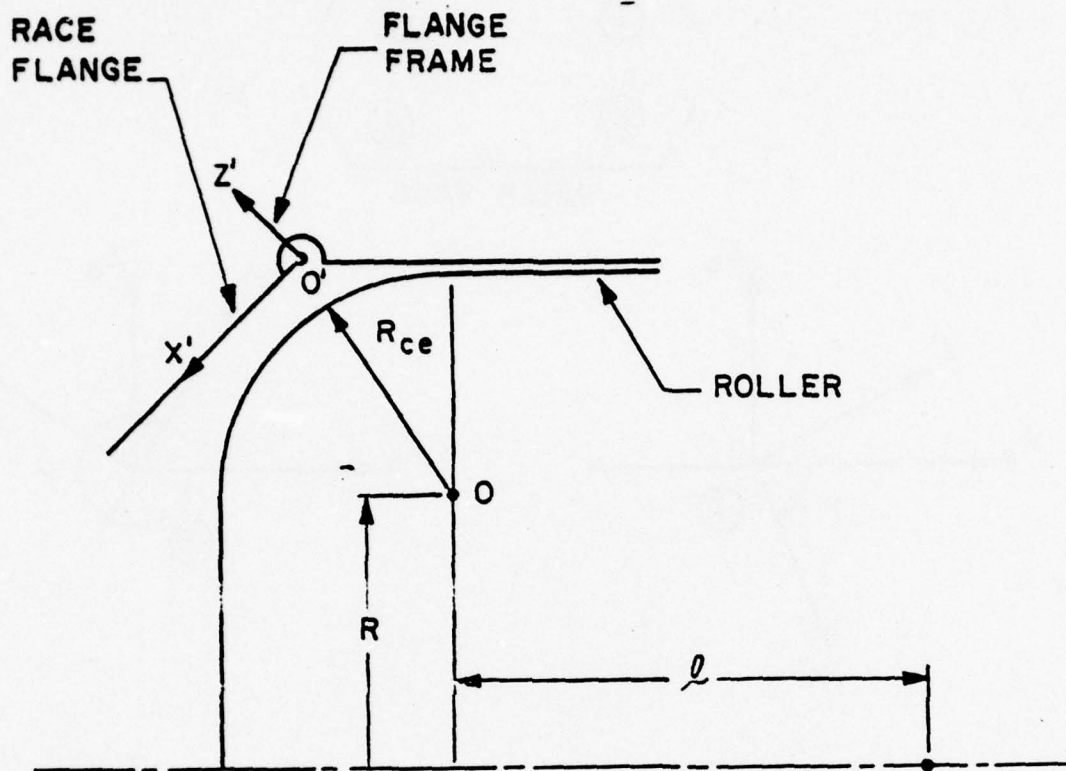


Figure IV-2. Exaggerated View of Roller Corner and Race Flange Interaction

Now for any selected value of ϕ in (IV.1), the race azimuth angle ψ is defined, such that the vector

$$\vec{r}_{er} = \vec{r}_e + \vec{r}_{brg}$$

when written in the race azimuth frame has only X and Z components. Hence,

$$\vec{r}_{er}^r = \vec{r}_{brg}^r + \{T_{br}\} \vec{r}_e^b$$

$$\text{and } \vec{r}_{er}^a = \begin{Bmatrix} r_{er1}^a \\ 0 \\ r_{er3}^a \end{Bmatrix} \quad (IV.4)$$

where

$$r_{er1}^a = r_{er1}^r \text{ and } r_{er3}^a = \sqrt{(r_{er2}^r)^2 + (r_{er3}^r)^2}$$

It should be remembered the \vec{r}_{er}^a locates the roller corner curvature center with respect to the race geometric center. If we define the point 0' as a reference point on the flange, then the roller curvature center can be referenced relative to 0' as

$$\vec{r}_{ef}^a = \vec{r}_{er}^a - \begin{Bmatrix} S \\ 0 \\ R \end{Bmatrix} \quad (IV.5)$$

where S is the race half width and R is the radius of the race land.

When the above is written in the flange frame

$$\vec{r}_{ef}^f = [T_{rf}] \vec{r}_{ef}^a \quad (IV.6)$$

Clearly, the point of maximum interaction will be determined by maximizing the Z component of \vec{r}_{ef}^f . In fact, the Z component will define the elastic deflection if it is positive, and greater than the corner radius, R_{ce} .

It may be recalled that all of the above is carried out for a preselected value

of ϕ in equation (IV.1). Thus, $(r_{ef}^f)_3$ is maximized by varying ϕ . Hence,

$$\frac{\partial}{\partial \phi} (r_{ef}^f)_3 = 0$$

After carrying out some routine algebra, it may be shown that the above equation may be written as

$$\begin{aligned} & T_{rf31} [-T_{br12} R \cos \phi - T_{br13} R \sin \phi] \\ & + \frac{T_{rf33}}{r_{er3}^a} \left\{ \sum_{i=2}^3 (r_{rr_i}^r + T_{br_{i1}}^2 - T_{br_{i2}} R \sin \phi + T_{br_{i3}} R \cos \phi) \right. \\ & \left. \times (-T_{br_{i2}} R \cos \phi - T_{br_{i3}} R \sin \phi) \right\} = 0 \end{aligned} \quad (IV.7)$$

The above is solved for ϕ by standard bisection. Note that there will be two possible roots, one denoting the maximum and the other defining a minimum. The interest here is, of course, in the maximum.

As discussed above, the elastic deflection will be defined by the $(r_{ef}^f)_3$ when it is positive.

$$\delta = (r_{ef}^f)_3 - R_{ce} \quad \text{when } > 0 \quad (IV.8)$$

If δ is negative, then there will be no interaction between the roller corner and the race flange.

Normal Contact Load

If the contact between the roller corner and race flange exists, then the contact load can be determined by using the classical point contact Hertzian solution described earlier (reference 2). Clearly, the deflection δ is computed as described above, the material properties are prescribed and the only additional parameters needed are the effective radii of curvature of the interacting bodies,

which may be defined as follows,

$$\begin{aligned} \text{Race flange} \quad & \begin{cases} R_1 = \infty \\ R_2 = R \end{cases} \\ \text{Roller corner} \quad & \begin{cases} R_1 = R_{ce} \\ R_2 = (R_{ce} + R) / \cos \theta_s \end{cases} \end{aligned}$$

where θ_s is the skew angle. This angle is included in the transformation T_{ib} used above and in the preceeding section.

It should be noted that when θ_s is zero, the above model will not be valid, since the entire end face of the roller will interact (for a flat end) and the contact is no longer Hertzian. Such a contact will only exists when there is a dominant thrust load on the bearing, which is never the case in cylindrical roller bearing.

An alternate way to compute the normal load will be similar to the one described for roller-cage and ball-cage interactions in (reference 1). A certain stress level for the computed deflection is prescribed and the contact area is just computed by the geometry of interaction.

Tractive Forces and Moments

The computation of tractive force will be very similar to the procedure described for the roller-race interaction presented in the preceeding section. The contact point is located relative to the roller and race mass centers and the slip velocities are computed. So, if \vec{r}_p^f defines the contact point relative to the roller mass center, and \vec{R}_p^f defines it relative to the race mass center, it will be straightforward to show that

$$\vec{r}_p^f = [T_{rf}] [T_{ra}] \left\{ \vec{r}_e^b + \vec{r}_{bg}^b \right\} + \begin{Bmatrix} 0 \\ 0 \\ R_{ce} \end{Bmatrix} \quad (IV.9)$$

$$\text{and } \vec{R}_p^f = \vec{r}_p^f + \vec{r}_{rr}^f + [T_{rf}] [T_{ra}] \vec{r}_{rg}^f \quad (IV.10)$$

where $[T_{ra}]$ is the transformation from the race frame to the race azimuth frame.

The local velocities at the contact point are clearly

$$\vec{u}_b = \vec{v}_b + \vec{\omega}_b \times \vec{r}_p$$

$$\vec{u}_r = \vec{v}_r + \vec{\omega}_r \times \vec{R}_p$$

$$\text{Effective slip } u_s = (u_{r_2} - u_{b_2}) \quad (\text{IV.11})$$

$$\text{and the traction coefficient } \kappa = \kappa(u_s) \frac{u_s}{|u_s|} \quad (\text{IV.12})$$

The total force acting on the roller is now defined in the flange frame as

$$\vec{F}_b^f = \begin{Bmatrix} 0 \\ \kappa Q \\ -Q \end{Bmatrix} \quad (\text{IV.13})$$

where Q is the normal contact load, discussed above.

The load of the race will just be

$$\vec{F}_r = - \vec{F}_b \quad (\text{IV.14})$$

and the moments on the roller and raceway will be

$$\vec{G}_b = (\vec{r}_p + \vec{r}_{bg}) \times \vec{F}_b \quad (\text{IV.15})$$

$$\vec{G}_r = (\vec{R}_p + \vec{r}_{rg}) \times \vec{F}_b \quad (\text{IV.16})$$

It must be remembered that all vectors must be transformed in appropriate coordinate frame. Generally, the forces will be computed in the inertial frame and the moments in the body fixed frame of reference.

SECTION V

ELASTOHYDRODYNAMIC TRACTION MODELS

Several approaches to a realistic model of the traction slip relationship of a given lubricant may be considered. The simplest approach will be to test the lubricant at the prescribed operating condition and derive a hypothetical model by curve fitting the experimental data. A somewhat more realistic approach will be to perform a two-fold elastohydrodynamic analysis where the first part will determine the nominal film thickness and the second part will evaluate the effective values of the coefficients in the pressure-temperature-viscosity relation by curve fitting the experimental traction data. A discussion of these different approaches is the primary objective of this section.

A Hypothetical Model

Most of the available experimental data shows a general trend demonstrated in Figure II-1. Traction initially increases with increasing slip, reaches a maximum value at some slip velocity, and finally reduces to some asymptotic value as the slip continues to increase further. Such a qualitative trend may be simulated by an expression of the form (reference 8)

$$\kappa = (\psi_1 + \psi_2 u) \exp(-\psi_3 u) + \psi_4 \quad (V.1)$$

where κ is the traction coefficient and u is the slip velocity.

In general, the coefficients ψ_1 , ψ_2 , ψ_3 , and ψ_4 will be a function of the operating conditions and the lubricant properties. However, if it is postulated that the model is valid for a given lubricant at prescribed operating conditions, then the values of the coefficients may be derived from the various parameters shown in Figure V-1, which can be expressed as

$$u = 0, \quad \kappa = \kappa_0 \quad (V.2a)$$

$$u = \infty \quad \kappa = \kappa_\infty \quad (V.2b)$$

$$u = u_m \quad \kappa = \kappa_m, \quad \frac{\partial \kappa}{\partial u} = 0 \quad (V.2c)$$

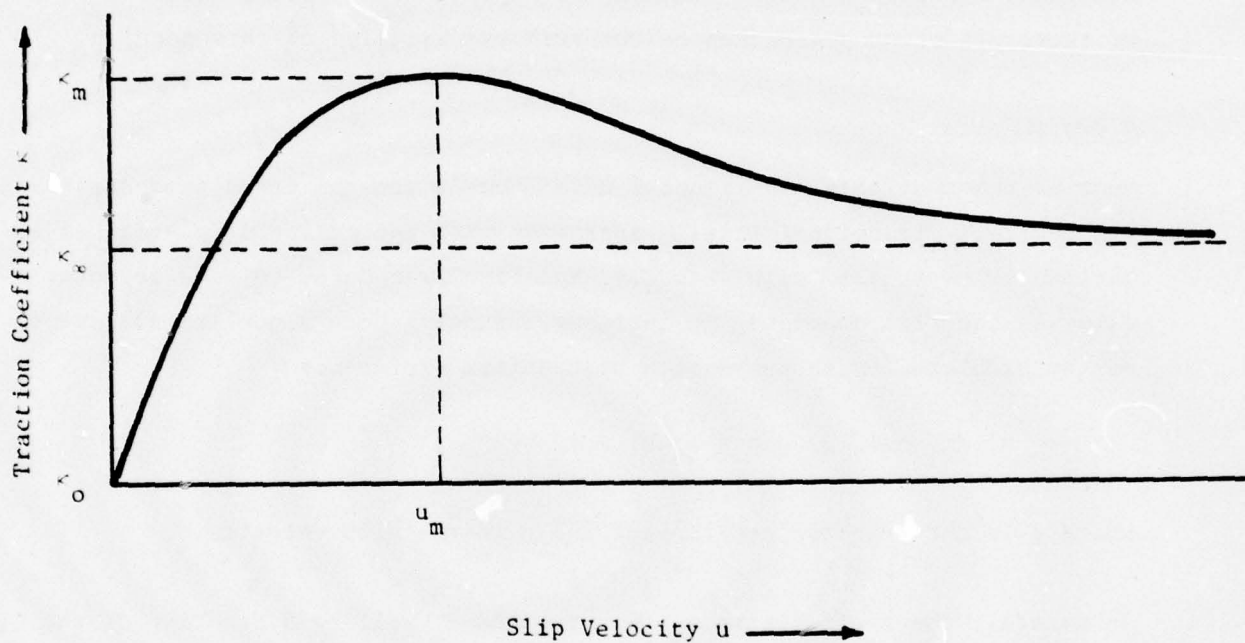


Figure V-1. Hypothetical Traction Slip Relationship

Combining (V.1), (V.2a), and (V.2b) gives

$$\psi_1 = \kappa_0 - \kappa_\infty \quad (V.3)$$

$$\psi_4 = \kappa_\infty \quad (V.4)$$

Also, from equations (V.1) and (V.2c)

$$-\psi_3 (\psi_1 + \psi_2 u_m) + \psi_2 = 0 \quad (V.5)$$

and

$$(\psi_1 + \psi_2 u_m) \exp(-\psi_3 u_m) + \psi_4 = \kappa_m$$

which form the two simultaneous equations for determining ψ_2 and ψ_3 .

Eliminating ψ_3 in equations (V.5) will give a nonlinear equation in ψ_2 .

$$(\kappa_0 - \kappa_\infty + \psi_2 u_m) \exp \left\{ - \frac{\psi_2 u_m}{\kappa_0 - \kappa_\infty + \psi_2 u_m} \right\} = \kappa_m - \kappa_\infty \quad (V.6)$$

which is solved by standard bisection methods. Hence, all the four coefficients can be computed from the prescribed conditions shown in Figure V-1.

It is clear that the above model is very simple in that it does not allow any variation in the parameter as a function of local variations in rolling speed, Hertz stresses, etc. In order to allow for these variations, a somewhat more sophisticated elastohydrodynamic model will be required. The first step in such a model is the computation of the nominal film thickness, which will be discussed below.

Nominal Film Thickness Computation

The computation of film thickness is one of the most fundamental steps in simulating the behavior of a concentrated elastohydrodynamic contact in rolling bearings. Most of the available analysis first determines the film thickness under isothermal conditions and the computed value is later modified by a thermal reduction factor in order to accommodate the thermal effects. Some of the formulae and computational procedures are discussed below.

Grubin Formula: This is perhaps one of the first relations which appeared in the literature (reference 9) for the computation of the isothermal film thickness h , in a line contact configuration

$$\frac{h}{R} = 1.95 \frac{(GU)^{8/11}}{W^{1/11}} \quad (V.7)$$

where

$$R = \frac{R_1 R_2}{R_1 + R_2}, \text{ the effective radius in rolling direction}$$

$$G = \alpha E', \text{ the elasticity parameter}$$

$$\frac{1}{E'} = \frac{1}{2} \left[\frac{1 - \nu_1^2}{E_1} + \frac{1 - \nu_2^2}{E_2} \right]$$

$$U = \frac{\mu_o \bar{U}}{E'R}, \text{ the speed parameter}$$

$$\bar{U} = \frac{1}{2} (\nu_1 + \nu_2), \text{ the rolling speed}$$

$$W = \frac{w}{E'R}, \text{ the load parameter}$$

ν , E , μ_o , α , and w are respectively the Poisson's ratio, elastic modulus, inlet viscosity, pressure viscosity coefficient, and applied load per unit length.

Dowson-Higginson's Formula: A similar relation is put forth by Dowson and Higginson (reference 9)

$$\frac{h}{R} = 2 \frac{G^{0.60} U^{0.70}}{W^{0.13}} \quad (V.8)$$

The various parameters are the same as these described in the case of the Grubin's formula.

Thermal Reduction Factor: The isothermal film thickness computed by any of the above expressions must be modified by a thermal reduction factor in order to allow for appropriate thermal effects. Cheng (reference 10) has summarized the results of a thermal analysis and the required thermal reduction factor can be computed by interpolating the results. Primarily for completeness, these results are reproduced here from reference 10.

The thermal reduction factor, ϕ_T , is expressed in terms of the following parameters

$$Q_m = \frac{\mu_o (v_1 + v_2)^2}{2 K_f T_o} = \frac{2\mu_o \bar{U}^2}{K_f T_o}$$

$$\alpha^* = \frac{\pi}{2} \cdot 10^5 \cdot \alpha$$

$$\beta' = \frac{\beta}{T_o}$$

$$s = \frac{v_2 - v_1}{v_2}$$

and $\frac{P_{Hz}}{E'}$, the dimensionless Hertzian pressure.

K_f , β , and T_o are the thermal conductivity, temperature viscosity coefficient, and inlet temperature, respectively. All other parameters are the same as discussed earlier.

The solutions of ϕ_T indicate that the most influential parameters are the viscous heating parameter Q_m . The other four parameters, α^* , β' , $\frac{P_{Hz}}{E'}$, and s all play secondary roles in governing the thermal reduction factor. In

particular, the influence of the slip ratio is very mild. A review of these curves shows that within the range of the parameters investigated, the thermal reduction factor can be represented by

$$\phi_T = f_1 (1 - 0.1 s) (1 - f_2 \frac{P_{Hz}}{E'}) \quad (V.9)$$

where f_1 and f_2 are numerical functions of Q_m , α^* , S' , and are tabulated in Tables V-1 and V-2.

Side Leakage Factor: Cheng (reference 10) has also presented a side leakage factor, ϕ_s , to modify the line contact film thickness in the case of elliptical contacts which may be relevant of crowned rollers. The dimensionless film thickness for an elliptic contact is expressed as

$$\frac{h_o}{R'} = C \left[\left(\frac{\mu_o \alpha U}{R} \right) \right]^{n_1} \left[\left(\frac{P_{Hz}}{E'} \right) \right]^{n_2} \quad (V.10)$$

where C , n_1 , and n_2 are numerical functions of a/b . These values are shown in Table V-3.

Assuming that the film thickness at $k = a/b = 5$ approaches that of a line contact, then the side leakage reduction factor becomes

$$\phi_s = \frac{C}{C_{k=5}} \left[\frac{\mu_o \alpha U}{R} \right]^{[n_1 - (n_1)_{k=5}]} \left[\frac{P_{Hz}}{E'} \right]^{[n_2 - (n_2)_{k=5}]} \quad (V.11)$$

The effective film thickness can now be expressed as

$$h = h_{iso} \phi_T \phi_s \quad (V.12)$$

TABLE V-1
VARIATIONS OF f_1 WITH RESPECT TO

$$\alpha^*, \frac{\beta'}{\alpha^*}, \text{ and } Q_m$$

$$(\alpha^* = \alpha \cdot \frac{\pi}{2} \cdot 10^5, \beta'/\alpha^* = \frac{\beta}{\alpha} \cdot \frac{1}{T_{o2} \frac{\pi}{2} \cdot 10^5})$$

α^* β' / α^*	15.71	15.71	15.71	23.564	23.564	23.56	31.419	31.419	31.419
Q_m	0.35	0.5	0.75	0.35	0.5	0.75	0.35	0.5	0.75
0.0	1.0	1.0	1.0	1.0	1.0	1.0	1.0	1.0	1.0
0.01	.99	.98	.99	.99	.97	.97	.98	.98	.98
0.02	.98	.96	.98	.98	.95	.94	.96	.95	.94
0.05	.96	.94	.93	.95	.92	.90	.93	.90	.89
0.1	.93	.9	.89	.9	.87	.84	.90	.85	.82
0.2	.89	.86	.81	.86	.81	.76	.84	.78	.74
0.5	.8	.78	.66	.77	.7	.62	.75	.66	.59
1.0	.72	.65	.56	.67	.6	.50	.66	.56	.46
2.0	.62	.53	.44	.57	.47	.36	.56	.45	.35
5.0	.47	.37	.3	.44	.32	.24	.43	.31	.23
10.0	.36	.27	.22	.34	.22	.17	.34	.21	.15

TABLE V-2
 VARIATION OF f_3 WITH RESPECT TO
 α^* , β'/α^* , and Q_m

$$(\alpha^* = \alpha \frac{\pi}{2} \cdot 10^5, \beta'/\alpha^* = \frac{\beta}{\alpha T \frac{\pi}{2} \cdot 10^5})$$

α^*	15.71	15.71	15.71	23.56	23.56	23.56	31.42	31.42	31.42
β'/α^*	0.35	0.5	0.75	0.35	0.5	0.75	0.35	0.5	0.75
Q_m	0.0	0.0	0.0	0.0	0.0	0.0	0.0	0.0	0.0
0.0	0.0	0.0	0.0	0.0	0.0	0.0	0.0	0.0	0.0
0.5	0.0	3.6	3.95	0.0	3.78	4.34	0.0	8.3	4.6
1.0	0.0	12.8	12.4	0.0	11.4	8.2	4.1	12.4	12.0
5.0	47.5	48.8	40.7	26.5	17.6	30.1	12.9	13.75	19.4
10.0	107.8	75.6	51.4	52.9	26.5	25.6	25.6	20.9	19.5

TABLE V-3
 NUMERICAL FUNCTIONS OF C , n_1 , AND n_2

$k = a/b$	C	n_1	n_2
5	1.625	0.74	-0.22
2	1.56	0.736	-0.209
1	1.415	0.725	-0.174
0.5	1.132	0.688	-0.066

The Turbo-33 Oil Model

Based on the experimental data (reference 11) on the Shell turbo-33 type oil, a traction model has been presented in reference 10. It is shown that the traction coefficient κ_2 , in the rolling direction is dependent on three parameters

$$G_1 = \frac{\mu_o u_2}{p_H h}; \quad G_2 = \frac{\beta_1 \mu_o u_2^2}{8K_f}; \quad G_3 = \alpha p_H \quad (V.13)$$

where μ_o is the lubricant viscosity at an inlet temperature of T_o ; K_f is the thermal conductivity of the lubricant; h is the film thickness; u_2 is the slip velocity in the rolling direction; p_H is the maximum Hertz pressure; and the coefficients α and β_1 are obtained from the viscosity-pressure-temperature model of the form

$$\mu(p,T) = \mu_o \exp [\alpha p - \beta_1 (T - T_o)] \quad (V.14)$$

The relationship between G_1 , G_2 , G_3 , and the traction coefficient κ_2 is represented graphically (reference 10) by a series of graphs and this data is basically stored in a computer data file for real applications. The film thickness h is computed by the methods described above.

With the assumptions of a narrow contact ellipse this model is directly applicable to a crowned roller contact. In equation (V.13), p_H is replaced by the pressure as a function of ξ

$$p_\xi = p_H \sqrt{1 - \left(\frac{\xi}{a}\right)^2}$$

and u_2 is clearly a function of ξ , the coordinate along the major axis of the contact ellipse (see Figure V-2). Thus, κ_2 is obtained as a function of ξ .

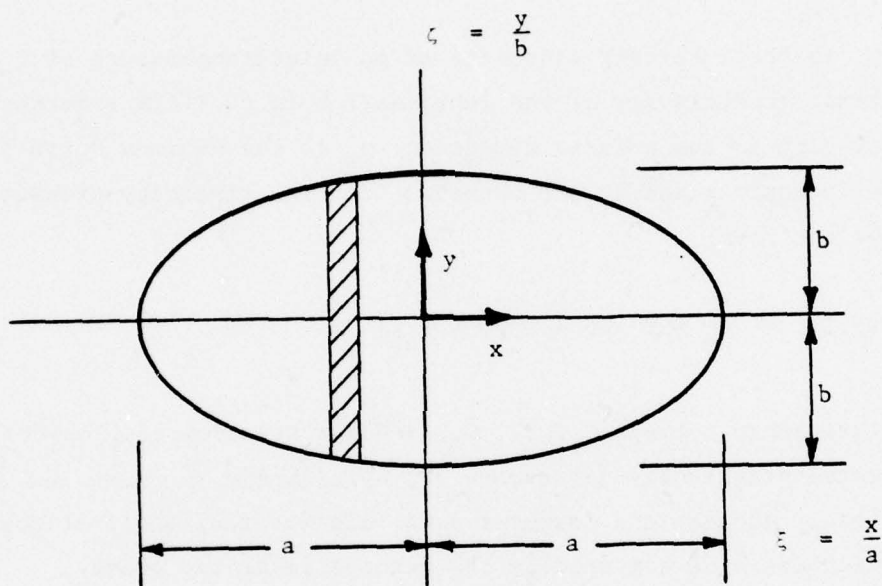


Figure V-2 Coordinate System in the Contact Ellipse

The 5P4E Polyphenyl Ether Model

Smith, et al (reference 12) have proposed a traction model based on the experimental data obtained by them for polyphenyl ether. It is shown that the shear stress in the lubricant is best correlated by an expression

$$\sigma_{\xi\zeta} = \frac{\mu_o u_2 \sin^{-1} [\psi \exp(\alpha^* p/2)] \exp(\alpha^* p/2)}{h \psi \sqrt{1 + \psi^2 \exp(\alpha^* p)}} \quad (V.15)$$

where

$$\psi = u_2 \sqrt{\frac{\mu_o \beta^*}{8K_f}}$$

p is the local pressure obtained by Hertzian pressure distribution, (ξ, ζ) is a coordinate system in the contact ellipse along the major and minor axes (see Figure II-2), and other parameters are the same as defined earlier. The three empirical constants, μ_o^* , α^* , β^* , denote the coefficients in a modified pressure-temperature-viscosity relation

$$\mu = \mu_o^* \exp \{ \alpha^* p + \beta^* (T - T_o) \} \quad (V.16)$$

and the value of these constants are determined by correlating the experimental data.

With the assumption of narrow ellipse equation (V.15) may be integrated with respect to ζ to obtain a tractive force per unit length along the major axis ξ . If this force is divided by the normal force per unit length, a traction coefficient κ_2 is the rolling direction determined. Some straightforward algebraic manipulation will show that

$$\kappa_2(\xi) = \frac{4}{\pi} \frac{\mu_o u_2}{h \psi^2 p_\xi} J(\xi)$$

where

$$J(\xi) = \int_0^1 \frac{\phi(\xi, \zeta) \ln [\phi(\xi, \zeta) + \sqrt{1 + \phi^2(\xi, \zeta)}]}{\sqrt{1 + \phi^2(\xi, \zeta)}} d\zeta \quad (V.17)$$

$$\phi(\xi, \zeta) = \psi \exp \left[\frac{\alpha \sqrt{1 - \left(\frac{\zeta}{b_\xi}\right)^2}}{2} \right]$$

and

$$b_\xi = b \sqrt{1 - \xi^2}$$

Generally the constants α^* and β^* are independent of rolling speed, while μ_o^* is allowed to vary slightly with the rolling speed in order to allow for the variation in traction as a result of short-time effects on lubricant viscosity or the inlet zone heating effects (reference 12). It is found (reference 12) that the values for the three coefficients which fit the experimental data are

$$\begin{aligned} \mu_o^* &= 1.4 \times 10^{-3} \text{ lbf-sec/in}^2, \text{ for rolling speed, } \bar{U} \leq 900 \text{ in/sec} \\ &= 1.4 \times 10^{-3} \exp \left\{ -0.30111 \left(\frac{\bar{U}}{900} - 1 \right) \right\} \frac{\text{lbf-sec}}{\text{in}^2}, \bar{U} > 900 \text{ in/sec} \\ \alpha^* &= 3.77 \times 10^{-5} \text{ in}^2/\text{lbf} \end{aligned}$$

and

$$\beta^* = 0.046 \text{ 1/}^\circ\text{R}$$

It should be noted that relation (V.16) is valid only for the computation of traction. For determining the film thickness a relationship of the form

$$\mu = \mu_o \exp \left\{ \alpha p + (\beta + \gamma p) \left(\frac{1}{T} - \frac{1}{T_o} \right) \right\} \quad (V.18)$$

is used, in which α , β , and γ are the conventional pressure-viscosity temperature-viscosity, and pressure-temperature-viscosity coefficients. For 5P4E polyphenyl ether, these constants have the following values.

$$\begin{aligned} T_o &= 630 \text{ }^{\circ}\text{R} & \mu_o &= 4.7489 \text{ lbf-sec/in}^2 \\ \alpha &= 1.1597 \times 10^{-4} \text{ in}^2/\text{lbf} & \beta &= 6.5042 \text{ }^{\circ}\text{R} \\ \gamma &= 0.18305 \text{ }^{\circ}\text{R lbf/in}^2 \end{aligned}$$

Using the above values, the inlet viscosity at any temperature can be determined. An additional property required in computing the thermal reduction factor is the thermal conductivity which is found to be $1.205 \times 10^{-2} \text{ lbf/sec/}^{\circ}\text{F}$.

The MIL-L-7808 Model

Similar to the polyphenyl ether model, Walowit and Smith (reference 13) have investigated the behavior of the MIL-L-7808 oil and have presented a traction model based on the experimental data. It is shown that the viscosity pressure temperature relationship, in the high pressure zone, for the purpose of computing traction is

$$\mu = 1.45 \times 10^{-7} \chi(\bar{U}) \exp \left\{ -9.949 + \frac{5.24719 \times 10^3}{T-345} - \frac{4.18935 \times 10^{-5}}{(T-345)^2} + 3.60 \times 10^{-5} p \right\} \quad (V.19)$$

where

$$\begin{aligned} \chi(\bar{U}) &= 1 \text{ for } \bar{U}, \text{ the rolling speed } \leq 900 \text{ in/sec} \\ &= \exp \left\{ -0.70320 \left(\frac{\bar{U}}{900} - 1 \right) \right\} \quad \bar{U} > 900 \text{ in/sec} \end{aligned}$$

and T and p are, respectively, the temperature ($^{\circ}\text{R}$) and pressure (lbf/in^2).

Using the above equation, traction is determined by simultaneously integrating the Newtonian shear and the energy equation through the film when the required boundary conditions are determined by the prescribed surface temperature and the rolling speed.

It turns out that such an integration has to be performed numerically and, hence, the model becomes somewhat time consuming. In view of this difficulty, equation (V.19) is further expanded to make it similar to (V.16), and coefficients similar to μ_o^* , α^* , and β^* are derived. These coefficients will now, of course, be functions of temperature and some straightforward algebra will show that the required expressions are

$$\begin{aligned}\mu_o^* &= \chi(\bar{U}) \cdot 6.92743 \times 10^{-12} \exp \left\{ \frac{5.24719 \times 10^3}{(T - 345)} - \frac{4.18935 \times 10^5}{(T - 345)^2} \right\} \frac{\text{lbf-sec}}{\text{in}^2} \\ \beta^* &= \frac{5.24719 \times 10^3}{(T - 345)^2} - \frac{8.37871 \times 10^5}{(T - 345)^3} \quad 1/^{\circ}\text{R} \\ \alpha^* &= 3.6 \times 10^{-5} \quad \text{lbf/in}^2\end{aligned}\tag{V.20}$$

$\chi(\bar{U})$ is the same as that described above in equation (V.19), and T will be the inlet temperature ($^{\circ}\text{R}$).

If the above values are used, then the 7808 model becomes identical to the polyphenyl ether model, except that the apparent coefficients, μ_o^* , α^* , and β^* are temperature dependent. The differences between such a simplified model and the actual model (reference 13) are shown in Figures V-3 and V-4 for some extreme cases. It is clear from these comparisons that the above approximations are quite reasonable.

This simplified approach also suggests that the general analytical approach can be used somewhat universally for any lubricant. It will be necessary to derive an equation similar to (V.19) and then, depending on the actual form of the equation, appropriate expansions may be substituted and relevant expressions for the apparent coefficients, similar to equations (V.20), may be derived. Once these coefficients are determined, the remaining analysis will be identical to that described in the case of the polyphenyl ether model.

Once again the pressure-temperature-viscosity relation of the form (V.18) is used for the computation of the film thickness. The low pressure viscosity data for the 7808 oil has been found to fit the following expressions (reference 14).

$$\mu_o = 1.45 \times 10^{-7} \exp \left\{ \exp (-3.7048 \ln T_o + 24.394) - 0.87 \right\} \frac{\text{lbf-sec}}{\text{in}^2}$$

$$\beta = \frac{3 \ln \mu}{3(1/T)} =$$

$$\frac{\exp [\exp (-3.7048 \ln t_o + 24.394)] \exp (-3.7048 \ln T_o + 24.394) 3.7048 T_o}{\exp [\exp (-3.7048 \ln T_o + 24.394)] - 0.87}$$

(V.21)

$$\alpha = 5.227 \times 10^{-6} + \frac{0.013332}{T_o - 388}$$

when T_o is the reference temperature ($^{\circ}\text{R}$).

Thermal conductivity of the MIL-L-7808 is found to be 1.2062×10^{-2} lbf/sec/ $^{\circ}\text{F}$.

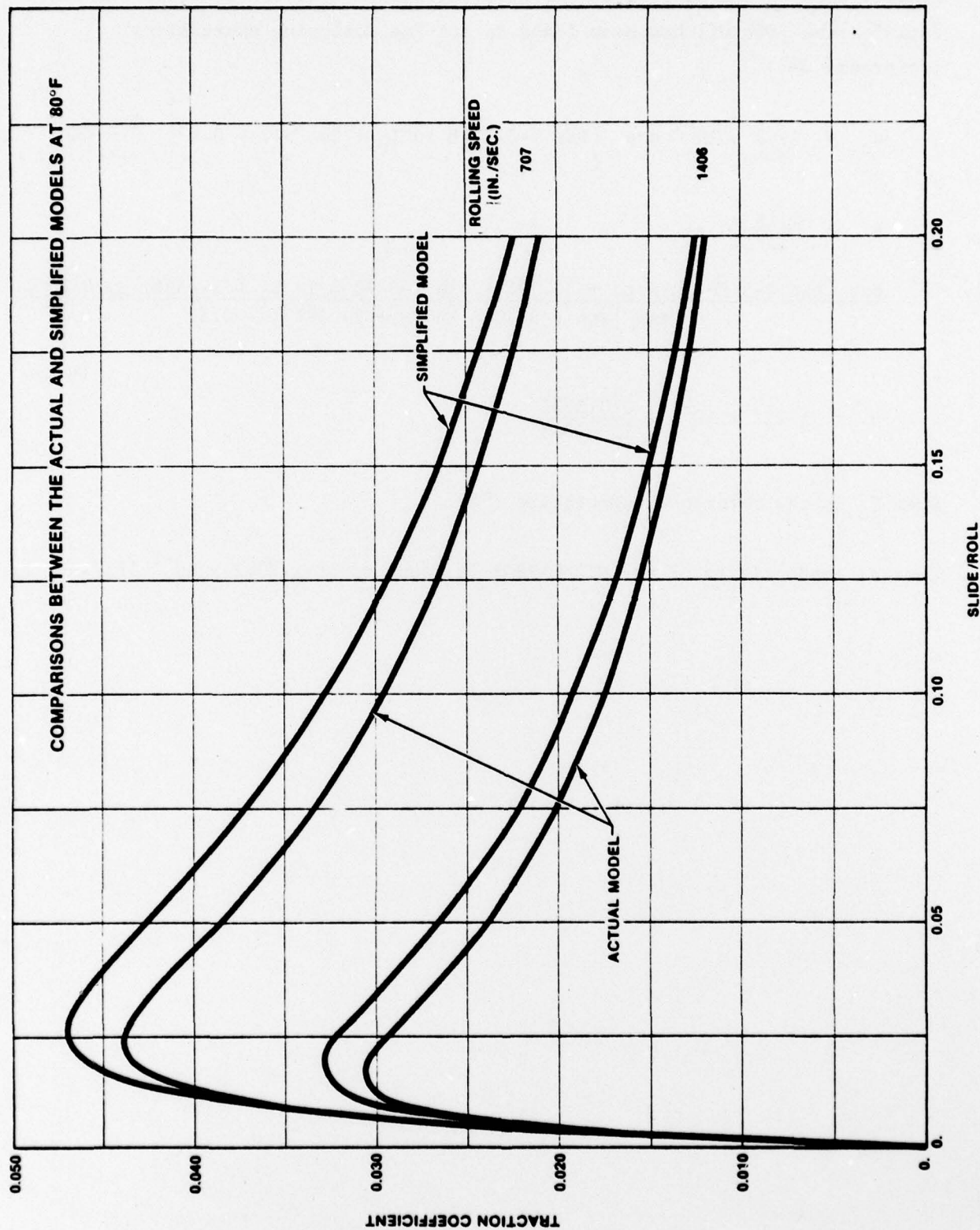


Figure V-3. Comparison of Actual and Simplified Traction Models
At $\dot{\gamma} / T\epsilon$ ratio

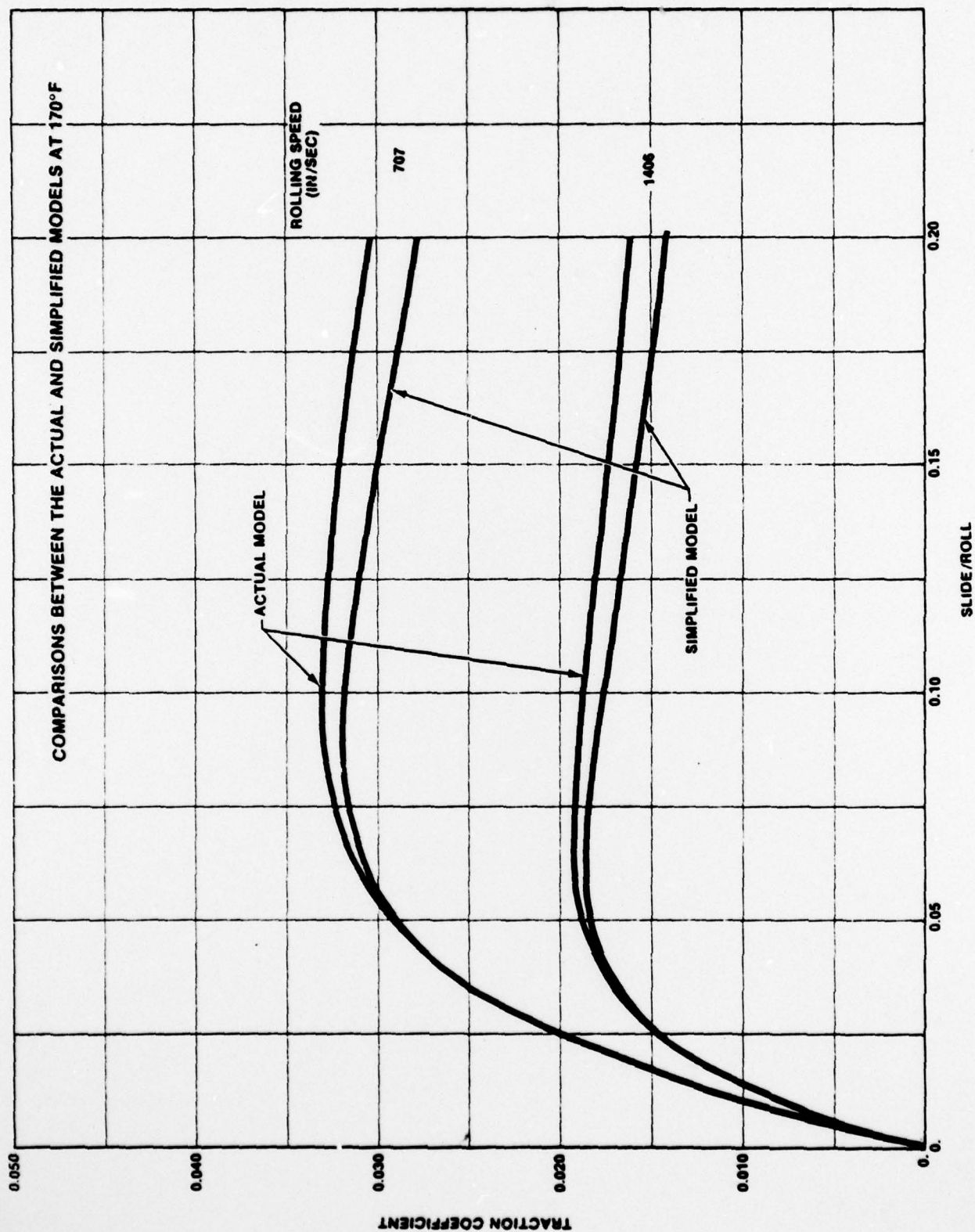


Figure V-4. Comparison of Actual and Simplified Traction Models At High Temperature

SECTION VI

ROLLER MOTION RESULTS

The analysis presented in the preceding section forms a basis for a roller bearing performance simulation computer program. This can be seen by examining some results for the roller motion in a typical high-speed roller bearing. Some geometrical details for the particular bearing are as follows:

Bore	6.49606 in.
Outside Diameter	8.858 in.
Roller Diameter	0.6299 in.
Roller Length	0.6299 in.
Central Flat Land	0.20 in.
Crown Radius	17.0 in.
Number of Rollers	32
Pitch Diameter	7.75 in.
Diametral Clearance	5.8×10^{-3} in.
Roller Corner Radius	0.050 in.

All the details about the cage geometry have been omitted since the emphasis is only on the roller motion in the present investigation.

The operating conditions assumed to be imposed on the bearing are:

Radial Load	1465 lbf
Inner Race Speed	13230 rpm
Outer Race Speed	0.
Inner Race Temperature	650°R
Outer Race Temperature	610°R
Lubricant	MIL-L-7808

In order to study the motion of a roller under the above condition, a simple

quasi-static type computation is first performed to determine the relative position of the races. As shown in Figure VI-1, the races are then held in this eccentric position and all the rollers are removed from the bearing. One roller is placed just before the start of the load zone with conditions identical to those in the full bearing. Using these conditions as initial conditions, the differential equations of roller motion are then integrated to simulate the general motion. Since such an integration is performed numerically, the equations are properly dimensionalized and the scales for the fundamental quantities are derived from the bearing geometry and applied conditions.

$$\begin{array}{llll}
 \text{Force} & = & \text{Applied Load} & = & 1465 \text{ lbf.} \\
 \text{Length} & = & \text{Roller Radius} & = & 0.3149 \text{ in.} \\
 \text{Time} & = & \sqrt{mr/Q} & = & 1.7495 \times 10^{-4} \text{ sec.}
 \end{array}$$

where m is the mass of the roller, r is the roller radius, and Q is the applied load.

The above quantities will also be used in dimensionalizing most of the results discussed below.

With reference to Figure VI-1, initially due to the centrifugal force, the roller is in contact with the outer race only. As it moves in the load zone, it comes in contact with the inner race and the load variation as the roller moves through the load zone is shown in Figure VI-2. The roller will experience radial accelerations due to this load cycle and also the resulting tractive forces will contribute to the orbital and angular accelerations of the roller. The general patterns of these accelerations are shown in Figure VI-3. The high frequency variations in the radial and orbital accelerations correspond to the roller/race contact spring resonance. In the load zone these will be both inner and outer race contact springs in parallel while only the outer race spring is relevant in the unloaded zone. Hence, the natural

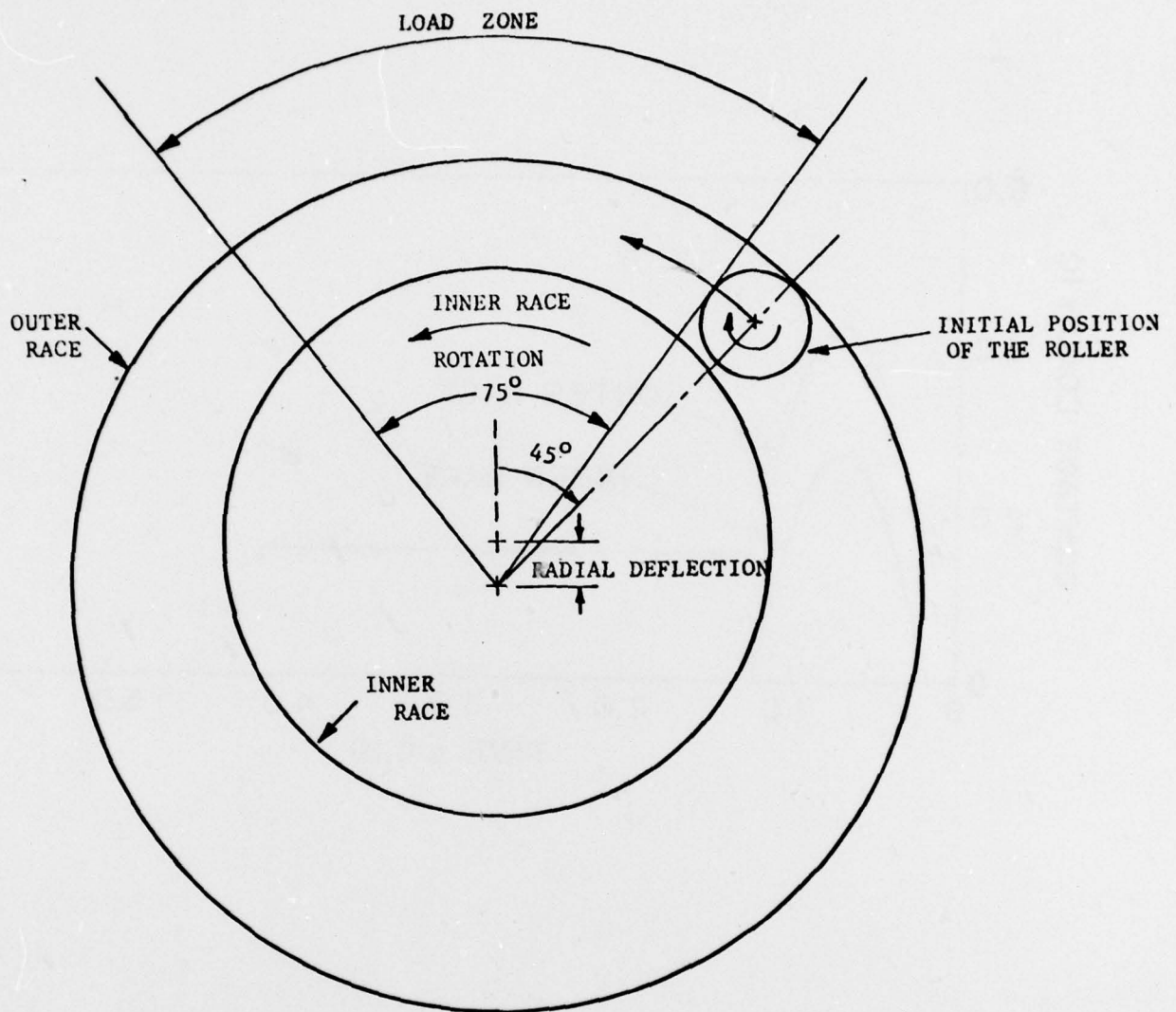


Figure VI-1. Exaggerated view of the bearing model used to study the roller motion

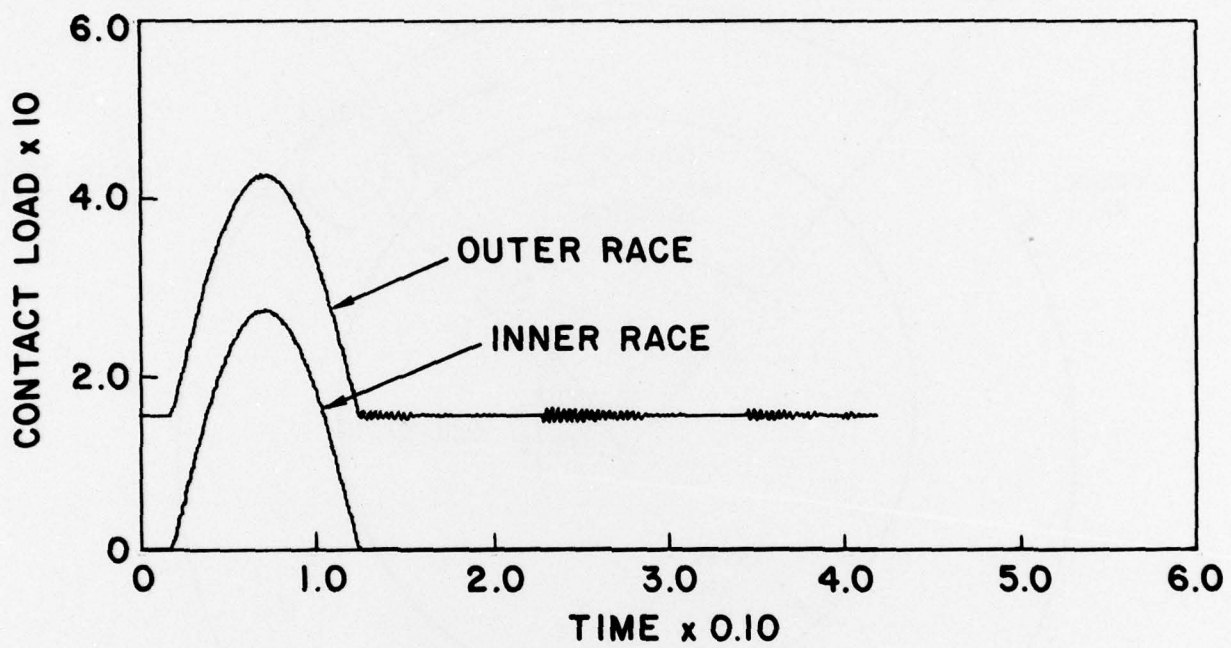


Figure VI-2. Roller/Race Contact Load Variation as the Roller Travels Through the Load Zone.

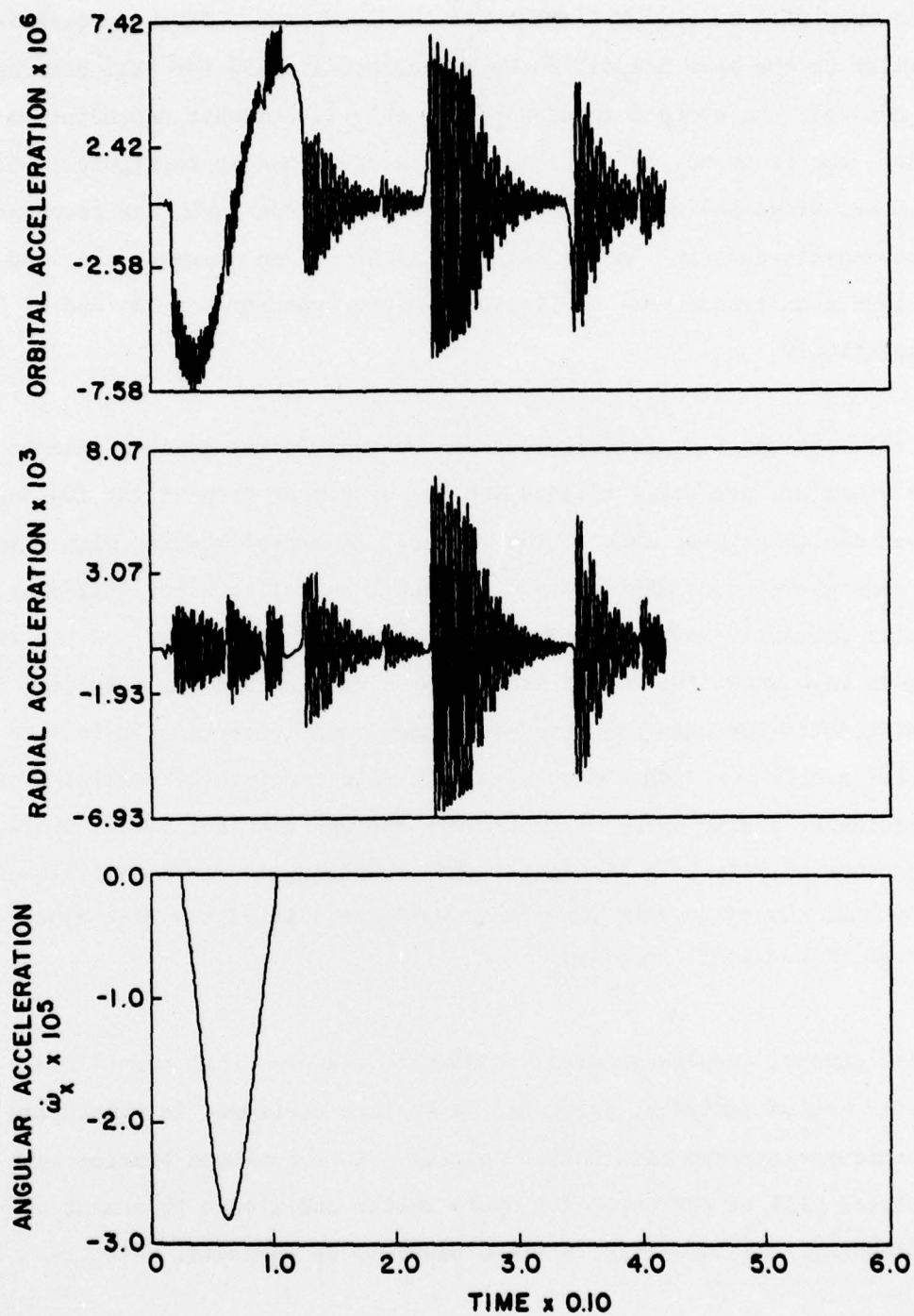


Figure VI-3. Typical Roller Acceleration Profiles as it Travels Through the Load Zone.

frequency will be somewhat higher in the load zone. These frequencies are similar to the ones identified by Gupta, et.al. [15] for ball bearings. In general, the contact resonance frequency is somewhat dependent on load. Hence, the frequency in the load zone is not constant in Figure IV-3. However, since the centrifugal force is fairly constant, the resonance frequency is constant in the unloaded zone. On an average, the load and no load zone frequencies in Figure VI-3 are approximately 24 and 17 kHz, respectively.

No skew type motion of the roller is observed in the present example, since the races are perfectly aligned and the system is free of any imposed moments about the transverse axis of the roller. In a real bearing with misalignment or some geometrical deviations will result in roller skew. Skidding of the roller primarily means relative sliding between the roller and the races. Figure VI-4 shows the roller/race slip velocities and the resulting traction coefficients for both the outer and inner race contacts. It is seen that the roller starts out with a zero slip (the selected initial condition) and it experiences a slip cycle as it travels through the load zone. Since the magnitude of slip is quite small, the traction curve is almost linear with slip and, therefore, the traction coefficients in Figure VI-4 appear to be almost proportional to slip.

These general results primarily summarize the practical significance of the roller motion analysis, presented in earlier sections, in simulating the dynamic performance of a roller bearing. In a complete bearing such an analysis will be performed for every roller and also a treatment of roller/cage and race/cage interactions will be included.

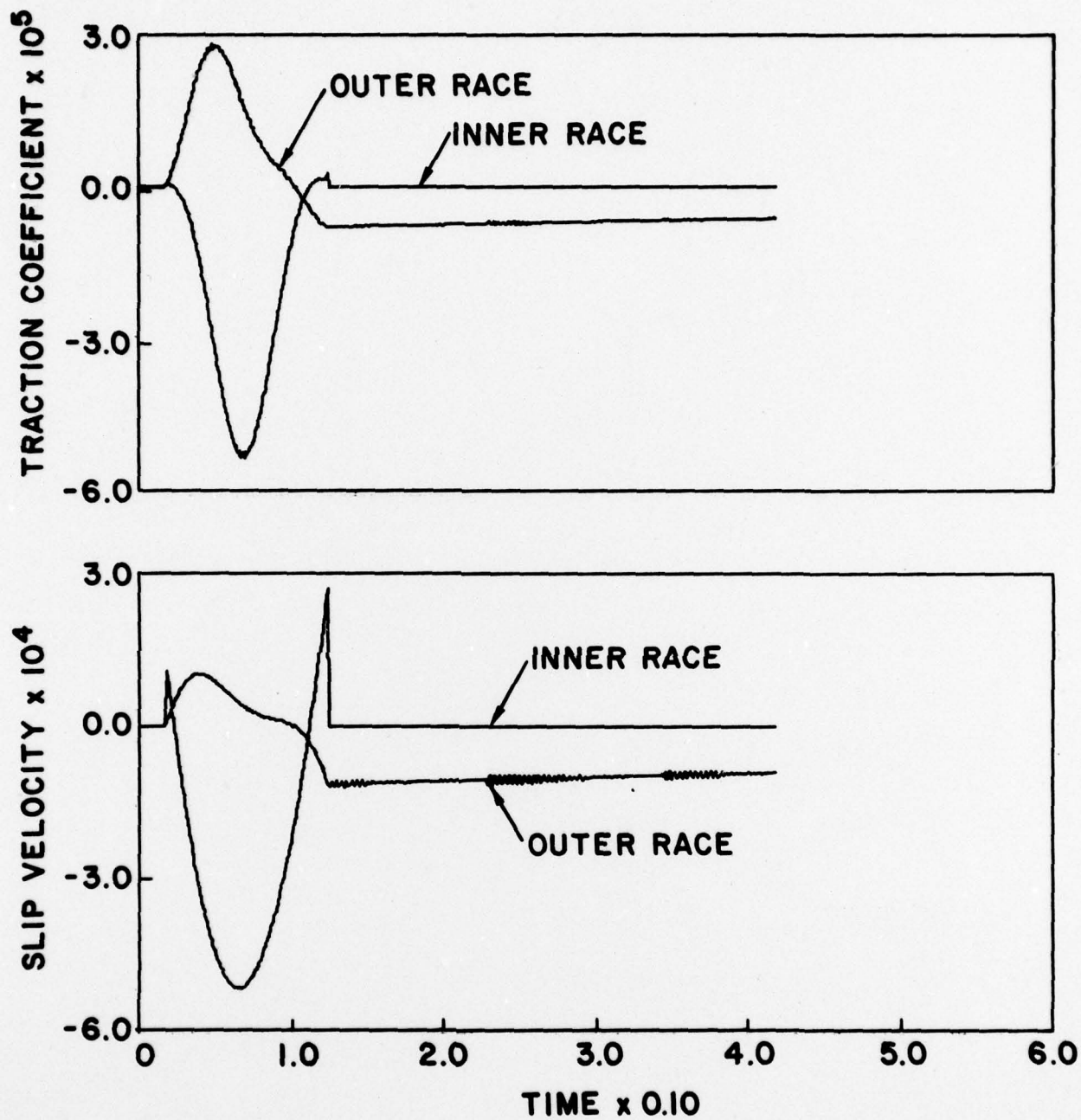


Figure VI-4. Roller/Race Slip and Traction Variations.

SECTION VII

SUMMARY

A generalized formulation of the differential equations of motion of a roller in a radially loaded cylindrical roller bearing is presented. The motion is considered in two parts, e.g., motion of the roller mass center in an inertial frame of reference and the angular motion about the roller mass center in a roller fixed coordinate frame. The formulation, therefore, has the complete six degrees of freedom and it has the capabilities of treating roller skew and other complicated, and often undesirable, motion. Also, the geometric formulation takes full account of any misalignment of the races.

Analytical frame work for the computation of applied forces and moments at the roller-race interaction is described. The normal contact force is primarily determined by locating the geometric center of the roller with respect to the interacting surface of the roller and, therefore, by computing the elastic deflection at the contact point. Knowing the deflection, the normal contact load is determined by the most commonly used Palmgren or Lundberg type of load deflection relation for a line contact. The tractive forces and moments are computed by first determining the local slip velocities in the contact zone and then estimating the traction coefficient from the given traction-slip model. The total contact zone is divided into several elements and the forces and moments are computed for each element and a proper summation is used to compute the total interaction. Thus, a full account for the local geometry, such as partial crowns, is taken.

In the case of roller skew the interaction between the roller corner and the race flange is considered. The general approach is very similar to that for the roller and race interaction described above. The position of the roller is located with respect to the race flange and the elastic deflection is determined by the geometric interaction. When no contact between the roller and flange exists, any hydrodynamic interaction is neglected, hence, only metal to metal contact is considered. The tractive forces and moments are determined by first computing the slip velocity and then using a specified traction slip relation.

Elastohydrodynamic traction models for three lubricants, the Shell turbo-33 oil, 5P4E polyphenyl ether, and the MIL-L-7808 oil, are presented in a form which is readily adaptable in the computerized simulations. All models are semi-empirical in nature and the characteristic coefficients are derived by curve fitting actual traction data obtained for a wide range of operating conditions. For bearings which have limited lubricant, relationships to modify the film thickness for starved conditions are presented and, hence, the influence of starvation on the traction characteristics, and ultimately the bearing dynamic behavior, is treated to a first approximation.

For a typical bearing the equations of motion are numerically integrated in order to examine the general nature of roller motion. It is shown that the radial acceleration of the roller mass center demonstrate the presence of a roller/race elastic contact resonance. This high frequency vibration results in variations in normal contact load; it also leads to corresponding variations in the tractive forces and, hence, the orbital accelerations. The general nature of roller/race slip variations, and the resulting traction coefficients, as the roller travels through the load zone is also simulated.

SECTION VIII

RECOMMENDATIONS FOR FUTURE RESEARCH

One of the primary findings of the present research has been that the roller is subjected to a high frequency motion resulting from roller/race resonance. Such a behavior should be confirmed experimentally. It is expected that these high frequencies will generally cause "ringing" of the outer race and, hence, their presence can be detected by picking up acceleration signals from the stationary race.

Roller skew and bearing misalignment are important subjects which can be studied by using the computer programs developed on the basis of the general roller motion presented in this report. Such a parametric study will be of a great practical and design significance.

SECTION IX

REFERENCES

1. Gupta, P.K., "Dynamics of Rolling Element Bearings - Part I: Analysis of Cage Motion", MTI Technical Report No. MTI-76TR42, June 1976.
2. Gupta, P.K., "Dynamics of Rolling Element Bearings - Part II: Analysis of Ball Motion", MTI Technical Report No. MTI-76TR44, July 1976.
3. Roark, R.J., FORMULAS FOR STRESS AND STRAIN, McGraw-Hill Book Co., 4th Ed., pp. 320.
4. Lundberg, G., "Elastische Berührung Zweier Halbkugeln", VDI Forschung, Vol. 10, No. 5, Sept/Oct 1939.
5. Palmgren, A., BALL AND ROLLER BEARING ENGINEERING, SKF Industries Inc., 3rd Ed., (1959).
6. Harris, T.A., ROLLING BEARING ANALYSIS, John Wiley, (1966).
7. Synge, J.L., and Griffith, B.A., PRINCIPLES OF MECHANICS, McGraw-Hill Book Co., (1959).
8. Kragelskii, I.V., FRICTION AND WEAR, Butterworth, 1965, pp. 178-184.
9. Dowson, D. and Higginson, G.R., ELASTO-HYDRODYNAMIC LUBRICATION, Pergamon Press, 1966, pp. 96-105.
10. McGrew, J.M., Gu, A., Cheng, H.S., and Murray, S. F., "Elastohydrodynamic Lubrication - Preliminary Design Manual", Wright-Patterson Air Force Base, Ohio, Technical Report AFAPL-TR-70-27, November 1970.
11. Johnson, K.L. and Cameron, R., "Shear Behavior of Elastohydrodynamic Oil Film at High Rolling Contact Pressures", Proc. Instn, Mech. Engrs., Vol. 182, London, 1967-1968, pp. 307-330.

12. Smith, R.L., Walowit, J.A., and McGrew, J.M., "Elastohydrodynamic Traction Characteristics of 5P4E Polyphenyl Ether", J. Lub. Tech., ASME Trans., Vol. 95F, July 1973, pp. 353-362
13. Walowit, J.A. and Smith, R.L., "Traction Characteristics of MIL-L-7808 Oil", J. Lub. Tech., ASME Trans, Vol. 98F, October 1976, pp. 607-612.
14. Smith, R.L., Walowit, J.A., Gupta, P.K., and McGrew, J.M., "Research on Elastohydrodynamic Lubrication of High Speed Rolling-Sliding Contacts", Wright-Patterson Air Force Base, Ohio, Technical Report AFAPL-TR-72-56, July 1972.
15. Gupta, P.K., Winn, L.W., and Wilcock, D.F., "Vibrational Characteristics of Ball Bearings", J. Lub. Tech., ASME Trans., vol. 95F, (1977) pp. 284-289.